IEEE Access
Multidisciplinary | Rapid Review | Open Access Journal

Received 25 September 2022, accepted 16 October 2022, date of publication 25 October 2022, date of current version 1 November 2022.

Digital Object Identifier 10.1109/ACCESS.2022.3216585

RESEARCH ARTICLE

Design and Synthesis of Ferrite Strip-Line Circulator Based on Enhanced Closed Form Solution and Power Handling Analysis

SOKHA KHIM[1], SOVUTHY CHEAB[2], (Member, IEEE), SOCHEATRA SOEUNG[1], (Member, IEEE), AND GUAN SHEN NG[1]

[1]Department of Electrical and Electronic Engineering, Universiti Teknologi PETRONAS, Seri Iskandar, Perak 32610, Malaysia
[2]FILPAL (M) Snd Bhd, Bayan Lepas, Penang 11900, Malaysia

Corresponding author: Socheatra Soeung (socheatra.s@utp.edu.my)

This work was supported in part by the Yayasan Universiti Teknologi PETRONAS, Universiti Teknologi PETRONAS, under Grant 015LC0-320; and in part by FILPAL.

ABSTRACT In this article, Y-junction strip-line circulators are designed using an enhanced closed form solution consisting of unified key equations and a flowchart design, which serves as a direct procedure for designing a ferrite circulator. This design methodology is combined with a 3D EM simulation that allows for the calculation of the saturation magnetization, uniform biasing, and ferrite dimensions needed for a circulator to operate in both modes. In addition, the closed form can be used to calculate the Y-junction parameters and allow the matching network to be calculated and the uniform circulator biasing design ended. Our analysis starts with the ferrite calculation to ensure that it is uniformly biased magnetically, and this is followed by strip-line design, Y-junction matching, and biasing circuit design. Using full-wave electromagnetic (EM), HFSS and magnetostatic (MS), Maxwell3D simulations, several key design parameters such as the saturation magnetization, coupling angle, and various external permanent magnetic biases are investigated. To validate the proposed concept, two strip-line circulators are designed and fabricated for operation in wide-bandwidth and narrow-bandwidth applications. Good agreement is found between the simulated and experimental responses for the S-parameters of the circulators. We also present a semi-analytical analysis of the concept of breakdown, which enables calculation of the peak power and total thermal rise in the strip-line structure. The average power handling capability of a strip-line circulator is studied for the first time. The proposed closed form expressions can also be implemented in various ferrite circulators using different guiding technologies for millimeter-wave applications.

INDEX TERMS Above resonance, below resonance, homogeneous, microwave ferrite, magnetostatic, non-reciprocal, splitting factor.

I. INTRODUCTION

Microwave ferrite circulators are passive three-port devices that are used in radio frequency (RF) applications whenever power needs to be directed to a specific point and isolated from another. The circulation condition for circulators, in which the RF signal flows in a circular way from one port and is attenuated in the reverse direction, arises due to the non-reciprocal properties of ferrite material. The basic operation of a circulator relies on magnetized microwave ferrite [1], [2], a ceramic material with non-reciprocal behavior, meaning that its behavior in one direction is very different from that in the other direction [3], [4], [5]. A circulator is an important microwave device that has been used in wireless communication, radar, satellite payload, medical, military and defense applications, laboratory measurements and industrial microwave heating. For example, a ferrite circulator is used in a base station tower where the transmitting and receiving chains share a common antenna, to isolate the receiver path from the transmitter path and vice versa.

The associate editor coordinating the review of this manuscript and approving it for publication was Photos Vryonides.

A circulator can be converted into an isolator by simply connecting a matched load to one specific port.

The conventional circulator design based on boundary conditions and a Green's function was reported in [6], [7], and [8]. An empirical analysis of a symmetrical quarter-wave coupled Y-junction strip-line circulator, described in terms of the counter-rotating mode, was presented in [9]. Ferrite circulator that employs the relations proved by both Bosma and Fay and Comstock can be found in [10], [11], [12], [13], [14], [15], [16], [17], [18], [19], [20], [21], [22], [23], and [24]. Circulators can be designed to operate either below resonance (BR) or above resonance (AR), depending primarily on the microwave operating frequency and the amount of biasing field applied. Thorough discussions of various aspects of circulator design, ranging from the properties of ferrite material to assembly and testing, are reported in [25], [26], [27], and [28]. Wideband circulators are known to be useful in communication systems, since the broadband emission-reception signals need higher bandwidth to provide faster communication. A wide bandwidth microstrip circulator was designed using a continuous tracking technique in [29]. Narrowband circulators are normally used at low frequencies where a high degree of isolation is needed. Research works on narrowband circulators using different guiding structures are found in [30], [31], and [32]. Despite the countless studies on the design and synthesis of ferrite circulators, the design of a circulator still deploys the same procedures based on empirical and iterative methods and has no exact design approach. A circulator design based on an empty substrate integrated coaxial line (ESICL) was reported in [33]. Although this is a novel technology, the authors used a trial-and-error method for synthesis, resulting in high costs and a time-consuming process.

Recently, there has been great interest in designing ferrite circulators using closed-form solutions. For instance, a disclosure design methodology based on a modified boundary condition and an expression for the closed form solution of the strip-line Y-junction was studied in [34] and [35]. The presented techniques can be considered an efficient method for circulator design, but they have several limitations: two unknown variables need to be estimated, a material with a high dielectric constant needs to be assumed, and most of the equations and state-of-the-arts were less simplified. In [36] a simplified flowchart for designing a microstrip baseline circulator was presented including a full-wave EM simulation. However, this approach was applicable to a microstrip baseline circulator, and the author explained much information regarding the effects of a permanent magnet.

More recent work [37] addressed some specific issues like the effect of ferrite thickness using field distribution. However, this work focused on high frequency, which is limited in fabrication, sensitivity physical dimension and material outsourcing. Most of the current research works mentioned above tend to apply to narrow bandwidth and no power handling capabilities were addressed in a good manner.

Power handling and waveguide circulators were studied in [38], [39], [40], [41], and [42]. Waveguide circulators have high power handling than strip-line circulators and suitable for high power application, but at low frequencies they become large structures and special mechanical design and multipaction analyses are needed to ensure proper operation and remove thermal energy from the materials [43], [44], [45], [46], [47]. More literature on power handling capabilities have been studied and applied for directional couplers, filters, and waveguide circulators, but not for Y-junction strip-line circulators [48], [49].

In this research, a modified closed-form solution with brief information and complete details along with a flow chart was proposed. These simplified closed-form equations and a flowchart for the design of a strip-line circulator that improves on the conventional circulator design can be applied to design both BR and AR circulators. An exact technical parameter of the ferrite and the Y-junction strip-line dimensions can be determined directly from this method. Unified circulator key design equations were also brought in together to assist the designing scheme as well as each equation and some rules of thumb were explained for proper understanding. In addition, the average power handling capability based on the thermal rise in the strip-line circulator is studied and validated using a complete computational fluid dynamics (CFD) solver for electronics thermal management called Icepak. The results of numerical calculations of the power handling of a 6–18 GHz circulator confirm those obtained from a full wave simulation. For instance, peak power of 870.23 W results in maximum field strength of 1.68 Mv/m in HFSS, which is slightly larger than half the breakdown voltage in air (3.22 Mv/m). And a maximum average power of 13.13 W corresponds to an operating temperature 85.20°C maximum from the Icepak simulation. Two circulators based on strip-line technology are designed, fabricated, and evaluated, and good agreement is shown between the simulation and experimental results.

II. UNIFIED CLOSED FORM SOLUTION

A. MICROWAVE FERRITE CALCULATION

Estimations of the required saturation magnetization ($4\pi Ms$) vary from one source to another. In the early stages of design of a ferrite circulator, there is no formula to derive the exact saturation magnetization. A suitable saturation magnetization should be based on a consideration of the lowest operating frequency [2]. The selection of an appropriate saturation magnetization mainly depends on the selected microwave frequency and the ferromagnetic resonance frequency. Three basic modes of operation will be considered, corresponding to the resonance, BR, and AR regions. The fractional [28] bandwidth of operation for both circulator schemes is mainly proportional to the selected saturation magnetization and bandwidth. Figure 1 shows a graph of the relationship between the loss performance and the biasing magnetic field. For instance, ''At low frequencies, the BR region becomes too

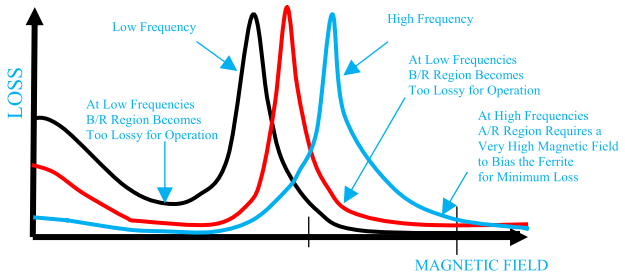

FIGURE 1. Variation in the region of operation with frequency [50].

lossy for operation", while "AR region becomes too lossy at high frequencies operation".

An estimation of the saturation magnetization can be calculated using (1), for both operating modes. The fractional bandwidth of the ferrite circulator is proportional to the saturation magnetization and inversely proportional to the differences in frequency. The bandwidth of operation can be calculated directly from (2) if the saturation magnetization has been chosen.

$$\frac{1}{2}\left(\frac{f}{\gamma}\right) - H_a \leq 4\pi M_s \leq \frac{4}{5}\left(\frac{f}{\gamma}\right) - H_a \tag{1}$$

$$\Delta f(\%) = \left(\frac{\gamma 4\pi M_s}{BW}\right) \times 100 \tag{2}$$

where γ is the gyromagnetic ratio (2.8 MHz/Oe)
f is the center or operating frequency in (Hz)
H_a is an isotropic field in the range (0–100 Oe)
BW is the operation bandwidth in (Hz)

Ferrite materials on the market typically have a saturation magnetization in the range of 90–5000 gauss and a resonance line width from 0.5–2500 oersted. They can operate between 0.02 and 94 GHz [4]. If we assume that the ferrite disk is saturated in the Z-direction, the elements of the permeability tensor can be expressed in Cartesian coordinates as [8]:

$$[\mu] = \begin{bmatrix} \mu & j\kappa & 0 \\ -j\kappa & \mu & 0 \\ 0 & 0 & \mu_0 \end{bmatrix} \tag{3}$$

where $\mu = \mu_0\left(1 + \frac{H_{in}4\pi M_s\gamma^2}{H_{in}^2\gamma^2 - f^2}\right)$ is the permeability tensor of the medium and $\kappa = \mu_0\left(\frac{f\gamma 4\pi M_s}{\gamma H_{in} - f^2}\right)$ is the off-diagonal element.

The permeability tensor elements κ and μ depend on the three main component f, H_{in} and $4\pi M_s$ which are known as the frequency of the microwave signal, the internal biasing field, and the saturation magnetization of proposed circulator properties, respectively. The effective permeability (μ_{eff}) and propagation constant in ferrite (κ_{eff}) can be defined using the following expressions [28]:

$$\mu_{eff} = \frac{\mu^2 - \kappa^2}{\mu} \tag{4}$$

$$\kappa_{eff} = \omega\sqrt{\varepsilon_f \mu_{eff}\varepsilon_0\mu_0} \tag{5}$$

Most modern circulators are designed for the first operation mode of circulation due to the need for miniaturization and to avoid complexity in the design equations. In the first mode, $n = 1$ or $x = 1.84$ the ferrite disk radius is given by [28]:

$$R_f = \frac{1.84\lambda}{2\pi\sqrt{\varepsilon_f \mu_{eff}}} \tag{6}$$

By substituting (5) into (6), we can get the ferrite radius as follows:

$$R_f = \frac{1.84C}{\omega\sqrt{\varepsilon_f \mu_{eff}\varepsilon_0\mu_0}} \tag{7}$$

where C is the speed of light in free space ($3 \times 10^8 m/s$) and ω is the radian frequency at circulation frequency (rad). The junction conduction, ferrite radius, ferrite thickness and loaded quality factor are related as modify [9]:

$$G_R d_f = 2.093\omega\varepsilon_0\varepsilon R_f^2\,(\kappa/\mu) \tag{8}$$

where Q_L and G_R are the approximate loaded quality factor and conductance of the ferrite resonator, respectively. The loaded quality factor is inversely proportional to the ferrite splitting factor (κ/μ) and is given by (9). The conductance of the resonator can be read from the graph in [28]. First, for the found range of Q_L and the maximum VSWR specification, we can use the value of G_R to find the ferrite thickness.

$$Q_L = \frac{1}{\sqrt{2}(\kappa/\mu)} \tag{9}$$

B. Y-JUNCTION STRIP-LINE DESIGN

Another variable that affects the bandwidth is the width of the inner conductor. It can be seen that the width of the tracing conductor used to guide the electromagnetic wave in the circulator is directly proportional to the coupling angle (ψ). This angle is limited to 120° apart from each other due to the nature shape of the Y-junction [26]. It takes two time of the coupling angle, which is (2ψ) to get the width of the strip-line Y-junction. Figure 2 shows the relationship between the Y-junction conductor and the width of the inner conductor. We first consider the disk geometry of the Y-junction, which has a diameter smaller than the ferrite disk. Most of the center conductors for Y-junctions are disk-shaped [9], [34]. There are certain advantages and disadvantages of each geometry in terms of the resonance frequency and engineering costs. In general, changes in geometry have only a weak effect on

Reference [26] but very large effects on B and G_R The selection of the center conductor geometry will depend on the shape of the ferrite and matching. Although, there is some room for adjustment regarding of on the choice. For instance, if it would be desirable to use a thinner or thicker ferrite, this can be accomplished by modifying the geometry of the center conductor [28]. It has been theoretically and experimentally proved that the diameter of the center conductor should be taken 80% of the disk resonator [51]. The wave admittance

of the circulator at the center frequency of operation is [9]:

$$G_R = \frac{Y_{eff}\,|\kappa/\,\mu|}{\sin(\psi)} \tag{10}$$

where Y_{eff} is the intrinsic wave admittance and is given in (11):

$$Y_{eff} = \sqrt{\frac{\varepsilon_f \varepsilon_0}{\mu_0 \mu_{eff}}} \tag{11}$$

From (10), we can derive the coupling angle based on the ferrite splitting factor in (4), the conductance of ferrite resonator can be derived from (10) and the intrinsic wave admittance in (11). The width of the Y-junction strip-line is calculated as follows:

$$W = 2R_C \sin(\psi) \tag{12}$$

where W is the inner width of Y-junction (mm)
ψ is the coupling angle (rad)
R_C is the center conductor radius (mm).

Figure 1 shows a configuration of Y-junction center conductor, which normally contains round center conductor and three strip-line arms. A small value of the coupling angle will result in wideband operation. Decreasing the coupling angle from light coupling ($\psi = 0.3$) to tight coupling ($\psi = 0.1$) will result in widening of the bandwidth operation, as Wu and Rosenbaum explained regarding their ''continuous tracking technique'' [9], which matches very well with measurement results in [52].

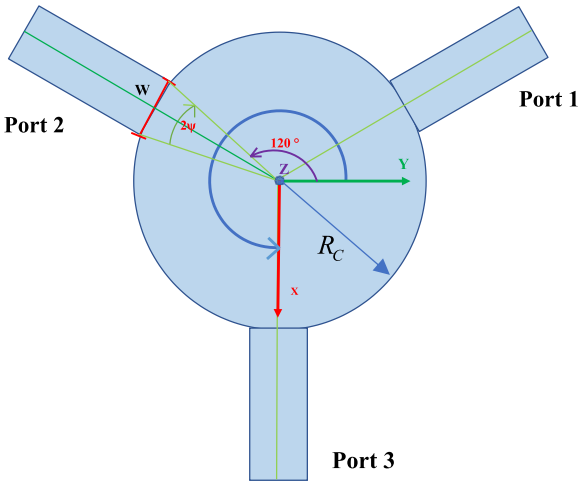

FIGURE 2. Configuration of the Y-junction strip-line.

C. CHARACTERISTIC IMPEDANCE OF THE Y-JUNCTION STRIP-LINE

A matched three-port Y-junction circulator provides perfect circulation (i.e., high isolation, low insertion loss, and wide bandwidth operation). The relationship between the characteristic impedance of the Y-junction circulator and ferrite splitting factor for wideband operation is explained in [29]. The wave impedance of a ferrite disk resonator and the wave impedance outside the disk can be determined as follows:

$$Z_{eff} = \frac{120\pi}{Y_{eff}\sqrt{\varepsilon_0}} \sqrt{\frac{\varepsilon_0}{\mu_0 \mu_{eff}}} \tag{13}$$

$$Z_d = \frac{120\pi}{\sqrt{\varepsilon_f}} \tag{14}$$

where Z_{eff} is the impedance of the ferrite resonator (Ω)
Z_d is the impedance outside the disk (Ω)
ε_f is the dielectric constant of the ferrite
ε_d is the dielectric constant of the surrounding medium.

Expressions for the effective diameter of the surrounding dielectric medium and the effective width of the supporting material of the strip-line are shown in (15) and (16), respectively.

$$R_e \approx R_f \sqrt{\left(1+\frac{4d_f}{\pi R_f}\right)\left[1-\left(4+5.2\frac{R_f}{2d_f}+1.45\frac{2d_f}{R_f}\right)^{-1}\right]} \tag{15}$$

$$W_e \approx W+\frac{2d_f-t}{\pi}\left[2a\ln(1+a)-(a-1)\ln(a^2-1)\right] \tag{16}$$

where $a = (1 - 0.5t/d_f)^{-1}$, $b \approx 2d_f$, and t is the thickness of the strip-line. Further on, the Z-parameters network of lossless, nonreciprocal, three-port network of circulator is well explained in [28] and [53]. Next, a matching circuit is designed to match the Y-junction impedance. Among the different matching techniques, a quarter wave-transformer is easy to design and match with other guiding structures. A research work of strip-line circulator with a numerical example matching procedure was addressed in [54]. The present of ferrite disc, which usually has input resistance below Y-junction strip-line (Z_0). To match ferrite disc to the standard system impedance, impedance transformer must be included. The characteristic impedance of the transformer for each section needs to satisfy the relation

$$Z_T^2 = Z_0 R_{in} \tag{17}$$

where $R_{in} = \mathrm{Re}(Z_{in})$ is the real part of the input impedance Z_R and Z_0 is 50 Ω. These transformers can have varying complexity and electrical size dependent on the desired performance and bandwidth. Other approaches to design strip-line could be used to obtain an optimum dimension. For instance, the results in [27] could be used, where key equations are explained in more detail.

D. CIRCULATOR BIASING

Circulators need an external biased field in order to cause the electrons in the ferrite to precess. It is very important that the magnetic field applied to the ferrite is uniform or homogeneous; otherwise, a portion of the ferrite may be only partly magnetized, or not magnetized. This situation leads to high insertion losses and generally poor circulator performance [28]. For a BR junction circulator, it is advantageous

to operate at a very low bias field with a magnetization (M) value that satisfies the relation

$$4\pi M < \beta\omega/\gamma \tag{18}$$

where β is a coefficient of about 0.5. At low bias fields, the ferrite is not fully saturated and (18) refers to the average magnetization ($4\pi M$) [7]. In the above resonance circulator, the external biasing magnetic field must be high enough to achieve low insertion loss and high isolation, yet low enough to cover the required bandwidth. The author of [8] reported that a good estimation for the biasing field for the above resonance circulator is at least four times the field that causes the ferrite to be saturated. However, the internal biasing field is in range from 1 to 5 times of saturation magnetization according to simulation. In another method of estimating the internal biasing for below resonance operation [34], the authors multiply the calculated saturation magnetization by a small coefficient. To summarize these two mentioned rules of thumb, the internal magnetic field (H_{in}) is estimated as follow:

$$H_{in} \approx 4\pi M_s(G) \times a \tag{19}$$

where a is the magnetic biasing constant. For example, a value of $a = 0.1$–0.5 could be used for a BR operation while $a = 2$–5 for an AR operation. To predict the optimum uniform biasing field in a ferrite circulator, the expression in (20) is applied:

$$H_{in} = H_0 + H_a - H_d \tag{20}$$

where H_0 is the applied external magnetic biased field (Oe)
H_a is the anisotropic field (Oe)
$H_d = N_Z 4\pi Ms$, where N_Z is the demagnetization factor of the ferrite sample. Normally, the demagnetization factor is estimated in the range (0-1) for non-ellipsoidal bodies. For example, the demagnetization factor of a disk-shaped ferrite has been reported as $N_Z = 0.88$ [11]. We can design a magnetic circuit using flux leakage [55] and alternative method with azimuthal symmetry in [56]. However, the design of magnetic circuits using these two methods is not exact and may be over-designed, which requires to use of a 3D simulation tool for tuning and optimization. The leakage factor F is defined as the ratio between the total magnetic flux density enclosed region. This magnetic flux leakage can be calculated using (21) followed by approximately magnet thickness as well its radius. In this work, we adopted the flux leakage method to design a magnet, that the detail is in section III.

$$F = 1 + \frac{1.7U_pL_g}{A_g}\left[\frac{L_p}{L_p+L_g} + 0.67\frac{0.67L_m}{0.67L_m+L_g+2L_p}\right] \tag{21}$$

where a subscript of p a property of the pole pieces if used, g denotes a property of the air gap, and m a property of the permanent magnets. U_p refers to the perimeter of the pole piece, L refers to height or length, and A refers to the area of the air gap at any point along the gap length. It is noted that the air gap can be replaced by ferrite in simulation.

$$L_g = (R_g + R_i)\left(\frac{A_m B_d}{FH_0}\right) \tag{22}$$

$$R_g = \frac{L_g}{\mu A} \tag{23}$$

$$A_m = \frac{FH_0A_g}{B_d} \tag{24}$$

where, R refers to the reluctance of a given path, R_g is the reluctance of the air or ferrite gap, and R_i being the reluctance of the flux return path. L, A and μ are the length of path, the cross-sectional area, and the relative permeability of the medium.

III. CAD-BASED DESIGN OF A STRIP-LINE CIRCULATOR

In this section, two strip-line circulators are designed and simulated using a unified closed-form expression and a simplified flow chart. Fig. 3 depicts a simplified flowchart for designing a ferrite circulator, from the specification stage through to evaluation, testing, and measurement. We divide the procedure into three stages. Fig. 3(a) shows a closed-form procedure for the design of a ferrite circulator with uniform biasing. Also figure 3(b) highlights the magnetic design and simulation in HFSS Maxwell3D. The prototype fabrication and sample materials purchasing are listed in Fig. 3(c). The proposed flowchart circulator design is summarized as the following procedure.

1) Determine the center frequency and fractional bandwidth from the specifications.
2) Derive for optimum saturation magnetization ($4\pi Ms$) using equation (1).
3) Estimate an internal biasing (H_{in}),Therefore, the elements of tensor can be found in using (3).
4) Determine preliminary dimensions of the ferrite circulator using equations (4) to (8).
5) Synthesize and simulate Y-junction strip-line to match 50-Ω load system impedance.
6) Perform 3D EM simulations under a uniform biasing field condition.
7) Design a static magnetic circuit for external magnet biased based on the assumption that we obtained the from point 6. This can be done with different methods. The flux leakage method is adopted in this work.
8) Add a pole piece, a spacer, and magnetic shielding to complete the magnetic circuit design with less discrepancy.
9) Calculate magnetic circuit thickness and diameter using flux leakage method and empirically iteration until it diverges
10) Performance magnetostatic simulation of the external biasing in Maxwell3D. The completed magnetic circuit can then be adjusted or optimized at this stage.
11) Couple a simulation between HFSS and Maxwell3D, by setup a link in a magnetic biasing source. Using excitation guidelines from Ansys's manual.

12) Carry out an optimization using the available tools in HFSS to obtain the best simulation results and provide some margin for the measurement stage.
13) Outsource and purchase ferrites, magnets, and other related materials from local or international suppliers.
14) Prepare the drawing for fabrication. The 3D drawing should save as a STEP file as a standard file for CNC machining.
15) Assembly all related components, compress and enclose casing properly.
16) Test and measure all related circulators' performance.
17) Fine-tuning pole pieces or magnets, by adding or removing them to get a good agreement result.

A. WIDE-BANDWIDTH 6-18 GHz STRIP-LINE CIRCULATOR

The design of the circulator begins with defining the operating frequency, bandwidth, and isolation. Here, A 6–18 GHz wideband circulator can be used for ultra-wideband radar applications, which occupies the X and Ku radio spectra. The specifications for the design of this wide bandwidth circulator are given in Table 1.

This wide-bandwidth circulator was designed based on an enhanced closed-form expression and flowchart as mentioned in section II. For instance, the saturation magnetization and fractional bandwidth can be estimated using (1) and (2) respectively. In this case, the saturation magnetization is calculated as $(4\pi M_s) = 4285.71$ gauss. However, the $4\pi M_s$ needs to multiply by a factor less than 1 to shift the bandwidth of operation slightly lower based on EM simulation. In this case, a new calculated saturation magnetization $(4\pi M_s)$ and fractional bandwidth (Δf) are then found to be 3500 gauss and 80% respectively. Using the equations (3)–(8), the ferrite electrical dimensions are calculated i.e., ferrite magnetic resonance frequency is $f_m = 2.8 \times 4\pi M_s$ (Hz), and resonance frequency $f_0 = 2.8 \times H_{in}$ (Hz). Considering the internal biasing field $H_{in} = 0$ Oe for below resonance operation. Resulting, $\mu = 1$, $\kappa = f_m/f_0 = 0.8166$ and therefore μ_{eff} and k_{eff} are calculated as $\mu_{eff} = (\mu^2 - \kappa^2)/\mu = 0.3330$ and $k_{eff} = \omega\sqrt{\varepsilon_f \mu_{eff}} = 561.75$ respectively. Next, assuming first mode of operation $x = 1.84$ therefore the ferrite radius is calculated as $R = 2.1361$ mm. By using the procedure in [28], the conductance and unloaded quality factor are calculated $G_R = 0.005$ and $Q_L = 0.0869$. Using (8), the single ferrite thickness $d_f = 1.562$ mm. Considering ferrite material that is suitable for achieving a wide bandwidth, we find that spinel ferrite is the best solution, as it has low insertion loss, high power handling and high curie temperature. In this design, a lithium spinel ferrite (XN36P) from Ningbov Chiyue [57] is used, and its technical parameters are shown in Table 2.

Using equations (9)–(11), we see that the Y-junction coupling angle is $\psi = 0.267$, while its width is then calculated as $W_1 = 0.565$ mm using (12). Then, assumed ground plan thickness is equal to two times ferrite height plus conductor thickness. Next, using (15) the effective radius of surrounding

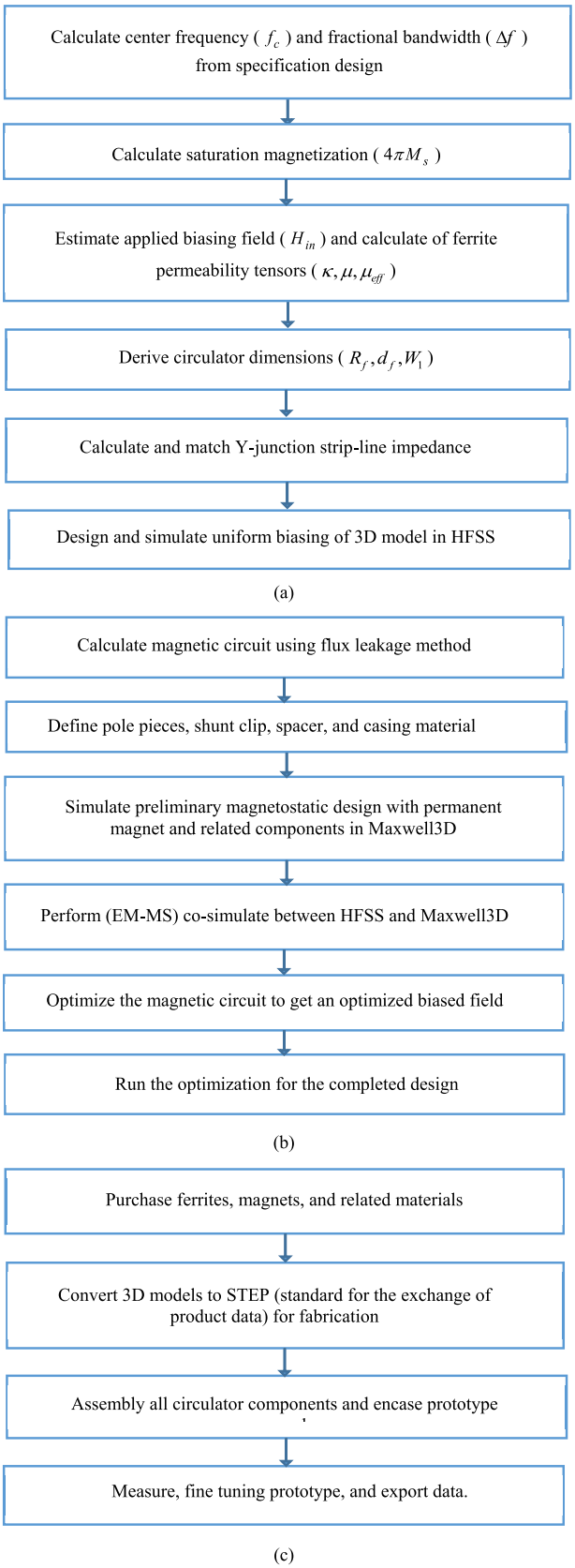

FIGURE 3. Proposed design procedure strip-line circulator: (a) closed-form procedure for designing a uniform circulator; (b) magnetic circuit design and simulation; (c) assembly and measurement.

TABLE 1. Design specifications for a 6–18 GHz circulator.

Specification	Value
Lower frequency	6 GHz
Upper frequency	18 GHz
Bandwidth	12 GHz
Insertion loss (IL)	1.2 dB
Isolation (IS)	13 dB
Return loss (RL)	12 dB

TABLE 2. Electrical parameters of ferrite.

Parameter	Value
Saturation magnetization ($4\pi M_s$)	3600 G
Resonance linewidth (Δf)	210 Oe
Ferrite dielectric constant (ε)	13
Land-g factor (g)	1.98
Ferrite radius (R)	2.136 mm
Ferrite thickness (d)	1.562 mm

dielectric is calculated to $R_e = 1.6834$ mm with center conductor diameter half of ferrite diameter. The standard load is 50 Ω, and the intrinsic wave impedance of the ferrite is found to be 56 Ω using (13). In this case, equation (17) is applied. Therefore, Z_R can be estimated by using another strip-line synthesis formula as explained in [27]. This strip-method could be used to design a 6–18 GHz wideband strip-line. And overall calculation can be summarized in the following procedure:

1) Assuming substrate thickness, conductor thickness, its conductivity, cavity height, dielectric constant of surrounding material, and loss tangent.
2) Calculate operating frequency. Setting impedance $Z_0 = 50\ \Omega$ and electrical length in degree (θ), and θ equal 90° for quarter wavelength transformer.
3) Use the characteristic impedance in (25) to find impedance with the found known W_e, b and ε_d from previous section.

$$Z_T = \frac{30\pi}{\sqrt{\varepsilon_d}} \frac{b}{W_e + 0.441b}. \tag{25}$$

4) To find the strip-line width, given the characteristic impedance (and assumption in point 1), which requires the inverse of (25). Such formula has been used as

$$\frac{W}{b} = \begin{cases} x & for\ \sqrt{\varepsilon_d} Z_0 < 120\ \Omega \\ 0.85 - \sqrt{0.6 - x} & for\ \sqrt{\varepsilon_d} Z_0 > 120\ \Omega \end{cases} \tag{26}$$

where

$$x = \frac{30\pi}{\sqrt{\varepsilon_d} Z_0}. \tag{27}$$

5) Calculate electrical length using equation (28)

$$l = \frac{C}{\omega\sqrt{\varepsilon_d}} \frac{\pi\theta}{180} \tag{28}$$

To get broadband operation, more than one section is inserted as per mentioned procedure. In this case, using a quarter-wavelength impedance transformer to match the Y-junction strip-line, its electrical dimensions can be seen in Table 3.

TABLE 3. Parameters of the 6–18 GHz Y-junction strip-line.

Parameter	Value
Center conductor radius (R_C)	1.068 mm
Inner width ($W1$)	0.565 mm
First section width ($W2$)	3.512 mm
Second section width ($W3$)	2.513 mm
Inner section length ($L1$)	0.743 mm
First section length ($L2$)	4.752 mm
Second section length($L3$)	1.151 mm

The 6–18 GHz strip-line circulator was simulated using ANSYS High-Frequency Simulation Structure (HFSS). Fig. 4(a) shows an exploded view of the various components used in a circulator. The strip-line is sandwiched between two ferrite resonators. Normally, a ferrite circulator contains magnets, spacers, pole pieces, ferrite, and a center conductor encased in one housing unit and a clip shunt, which acts as magnetic shielding. In Fig. 4(b), a 3D view of the wideband circulator, in which Sub-Miniature Version A (SMA) connectors are attached to the body of the circulator. Fig. 4(c) shows a view of the Y-junction strip-line of the 6–18 GHz circulator.

The saturation magnetization of ferrite is found to be critical for the design of the wide-bandwidth circulator. Using the key design equation in (1), the value of the saturation magnetization can be estimated as $(4\pi M_s) = 4185.71$ G. Figure 5 shows the S-parameters for different values of the saturation magnetization. At high saturation magnetization $(4\pi M_s) = 4200$ G, insertion loss (S_{21}) at higher side drops down below 1 dB, which considers high loss. The isolation (S_{31}) and return loss (S_{11}) are 11 dB and 12.5 dB covered frequency range (7–18 GHz). When we slightly decrease the saturation magnetization to $(4\pi M_s) = 3800$ G, the frequency is shifted upwards, out of the required bandwidth. The insertion loss (S_{21}) slightly decreases to 1.1 dB for the upper side band. At a value of $(4\pi M_s) = 3500$ G, a good insertion loss (S_{21}) around 1dB is achieved. Return loss (S_{11}) and isolation (S_{31}) are 14 dB and 12.5 dB respectively in the range (7–18 GHz). The fractional bandwidth almost 80% is obtained in the simulation.

The most challenging aspect of designing a wide bandwidth circulator is the design of the matching circuit. Impedance matching is used to match the ferrite impedance to the Y-junction strip-line. Selecting the right ratio between the ferrite radius and center conductor also helps in defining the matching. Normally, for a wide-bandwidth circulator, the center conductor is calculated as 50% or 80% of the ferrite radius, although it is sometimes selected to be the same as the ferrite radius. The inner width of the Y-junction strip-line also plays an important role in the matching circuit in terms

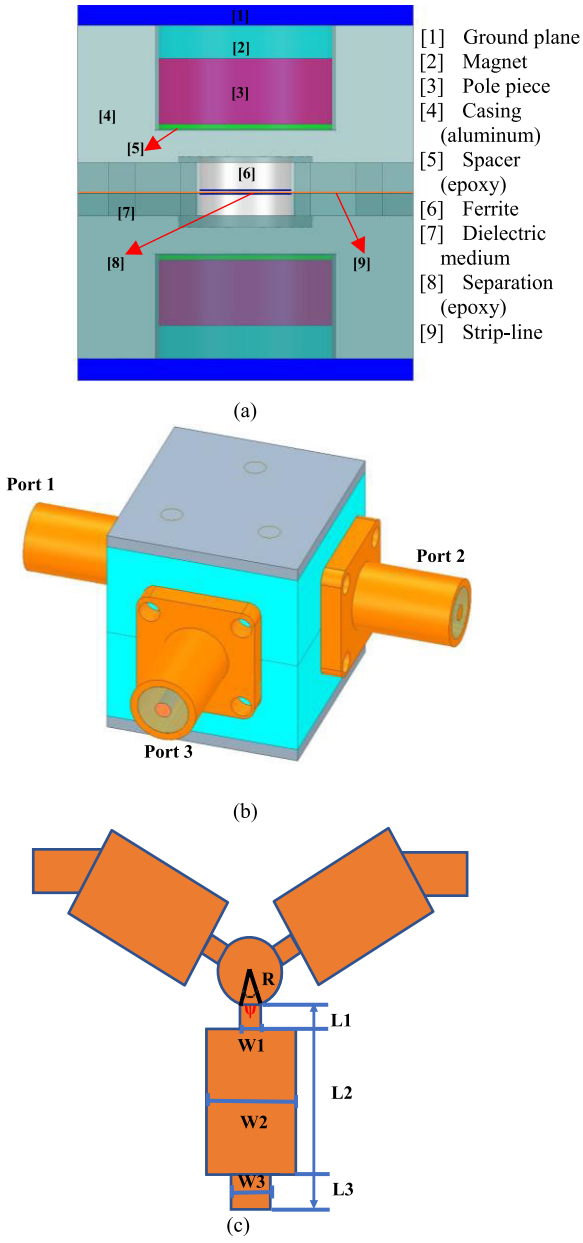

FIGURE 4. Design of the 6–18 GHz Y-junction strip-line circulator: (a) front view with detail of ferrite circulator components; (b) HFSS 3D view; (c) configuration of the 6–18 GHz Y-junction strip-line.

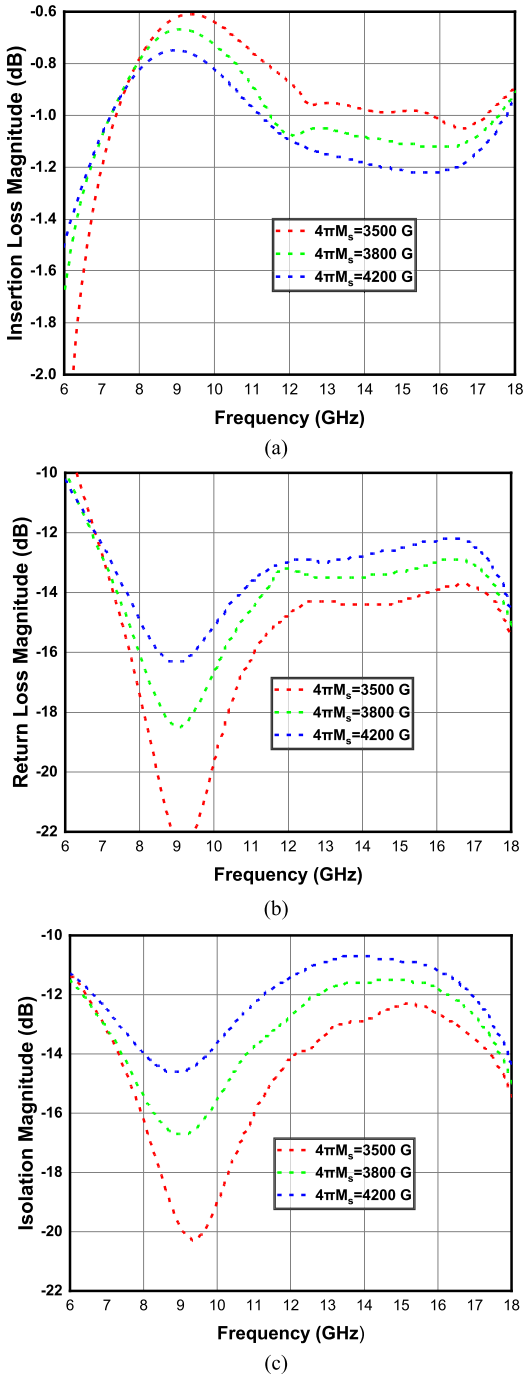

FIGURE 5. Graphs of the simulated S-parameters for different values of the saturation magnetization: S_{21}; (b) S_{11}; (c) S_{31}.

of maintaining wideband operation and good isolation at the center frequency. The calculated inner strip-line width is directly proportional to the coupling angle, as shown in (12). Figure 6 shows the scattering parameter of the strip-line circulator with varying coupling angle. For a light coupling angle ($\psi = 0.26$ rad), the insertion loss (S_{21}), return loss (S_{11}), and isolation (S_{31}) are 1.1, 13, and 12 dB respectively, at the center frequency of 12 GHz. As the coupling angle becomes tighter (i.e., increases), the return loss (S_{11}) and isolation (S_{31}) increase, while insertion (S_{21}) decreases. If the coupling angle is increased further, the insertion loss at the upper side frequencies will increase simultaneously, while providing an isolation (S_{31}) and return loss below 15 dB for the covered bandwidth (9–18 GHz). The main problem at this stage is to design an optimum magnetic biasing circuit. The selection of the type of magnet and its size or weight is also important at the design stage. The magnitude of the magnetic field together with the maximum size, weight, material properties, surface coating and weight are the key factors in the selection of the magnet. The magnets commonly used in circulators fall into four broad classes: ceramic (barium or strontium ferrite), alnico (aluminum-nickel-cobalt), samarium cobalt, and

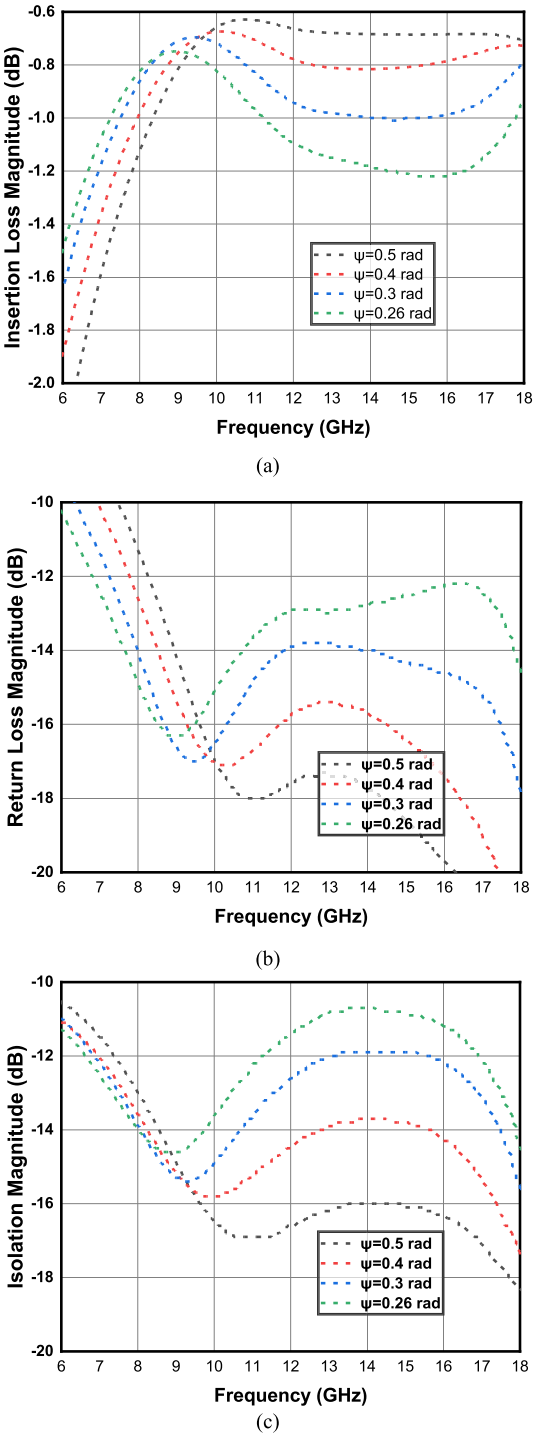

FIGURE 6. Graphs of the simulated S-parameters for different values of the coupling angle: (a) S_{21}; (b) S_{11}; (c) S_{31}.

neodymium-iron-boron. A weak biasing field is insufficient to bias a ferrite, and results in an incorrect bandwidth and an out-of-resonance frequency for the ferrite resonator. A strong biasing field will lead to a high magnetic loss or will tend to narrow down the bandwidth.

To obtain the optimum and actual environment biasing, an external permanent magnet is used to provide a biased field. The field from the magnet makes the circulation of non-reciprocal ferrite happen. By referring to the flux leakage method mentioned in section II and using Ansys Maxwell3D, two permanent magnets are calculated and simulated. First, we define the working air or ferrite gap, which normally equals 2 times ferrite thickness. Also, ferrite diameter is picked up the based-on design. Therefore, its area can be calculated. Second, we should set the pole piece thickness and calculate its perimeter. Third, we select $\mu = 4000$, which is the relative permeability of iron. Four define the working total path length and its area. And calculate the reluctance of each medium. Fifth, based on the BH curve of the permanent's datasheet, find B_d and H_d, where the maximum energy product of the magnet is located. In this case, neodymium-iron-boron 35 grade (NdFeB-N35) is used. BH's curve of this magnet shows $B_d = 6.5$ kG and $H_d = 6.2$ kOe respectively. Now, begin iteration of flux leakage until it becomes diverges at some point. And one should notice that there are two available options from (22) for iteration calculation one is to fix magnet thickness and vary its radius and another one is the opposite. In the first iteration, magnet thickness is calculated $L_m = 0.115$ and flux leakage is then calculated $F = 1.270$. Next, we set $A_m = A_g$ then $B_d = FH_0$ is derived from flux leakage at the first iteration.

So, the following iteration will continue by following the same procedure until diverge. An empirical iteration of this magnet is shown in Table 4. Finally, a neodymium-iron-boron grade N35 (NdFeB-N35) magnet from SDM Magnetics Co.Ltd, [58] is selected for this circulator, and its technical properties are listed in Table 5.

TABLE 4. Empirically iteration calculation of NdFe-N35 magnet.

Iteration	L_m (inch)	F	B_d (G)	H_d (Oe)
1	0.115	N/A	6500	6200
2	0.117	1.270	2700	6100
3	0.123	1.271	2758	5800
4	0.122	1.272	2762	5890

TABLE 5. Technical properties of neodymium-iron-boron grade N35 for a BR circulator.

Parameter	Value
Intrinsic coercive force (H_{ci})	12 kOe
Residual induction (B_r)	11.8 kG
Grade	N35
Maximum energy product ($BH_{\max}$)	35 MGOe
Curie temperature (T_c)	350 $^{\circ}C$
Maximum operating tempearute (T_m)	80 $^{\circ}C$
Magnet diameter (D)	4.22 mm
Magnet thickness (d)	1.52 mm

This external magnetic circuit is simulated in Ansys Maxwell3D using an axially magnetized disk permanent magnet, as shown in Fig. 7. The figure also shows that the

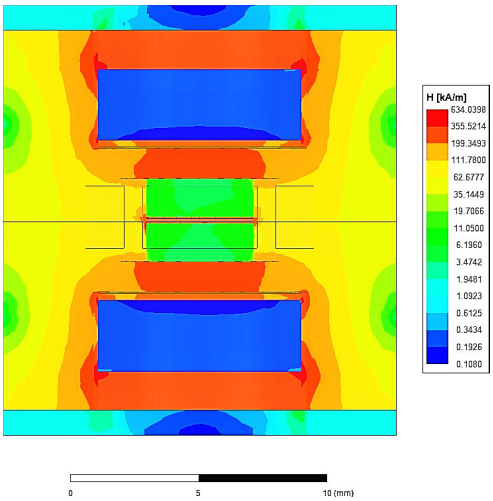

FIGURE 7. Simulated magnetic circuit generated by NdFeB-N35.

maximum simulated DC biasing field is 634.03 kA/m for below resonance operation.

After a large set of simulations and optimization, the optimum values of the Y-junction strip-line circulator are shown in Table 6. Figure 8 (a) shows a comparison between the initial design and optimized simulation S-parameter response of the wideband circulator at a center frequency of 12 GHz. An isolation (S_{31}) is below 14 dB in range of 7.55–18 GHz in optimized simulation. An optimum isolation at each port to the next adjacent port of the circulator can be found in Fig. 8 (b). Circulators are known as non-reciprocal passive devices, that is mean is meant that their behavior is nearly the same at each port. Theoretically, isolation from port 1 to port 3 (S_{31}) is equal to isolation from port 2 to port 3 (S_{23}), and isolation from port 1 to port 2 (S_{12}). In the simulation, all isolations show a little discrepancy regarding on small mismatch at each port. Figure 4(c) depicts an insertion phase difference among ports of the wideband circulators. This parameter is defined as the deviation from a best fit straight line of insertion phase versus frequency. For BR and AR circulators with less than 20% bandwidth, the phase linearity will generally be within 2 degrees [50]. In this case, the simulated insertion phase difference among ports of this wideband circulator is about 7 degrees, which operating bandwidth up to 80%. It is noticed that the insertion phase of port 1 to port 3 (S_{31}) and the insertion phase of port 2 to port 1 (S_{21}) nearly overlap, while the other port (S_{23}) drastically shifts about 7 degrees above its counterpart.

B. NARROW-BANDWIDTH 1.4–1.6 GHz STRIP-LINE CIRCULATOR

In this section, we design a narrow-bandwidth circulator with a frequency range [1.4–1.6 GHz]. The proposed narrowband circulator operates in the L-band spectrum, which is used by various applications such as radar, digital audio broadcasting, and global positioning systems. The design specifications of the circulator are summarized in Table 7.

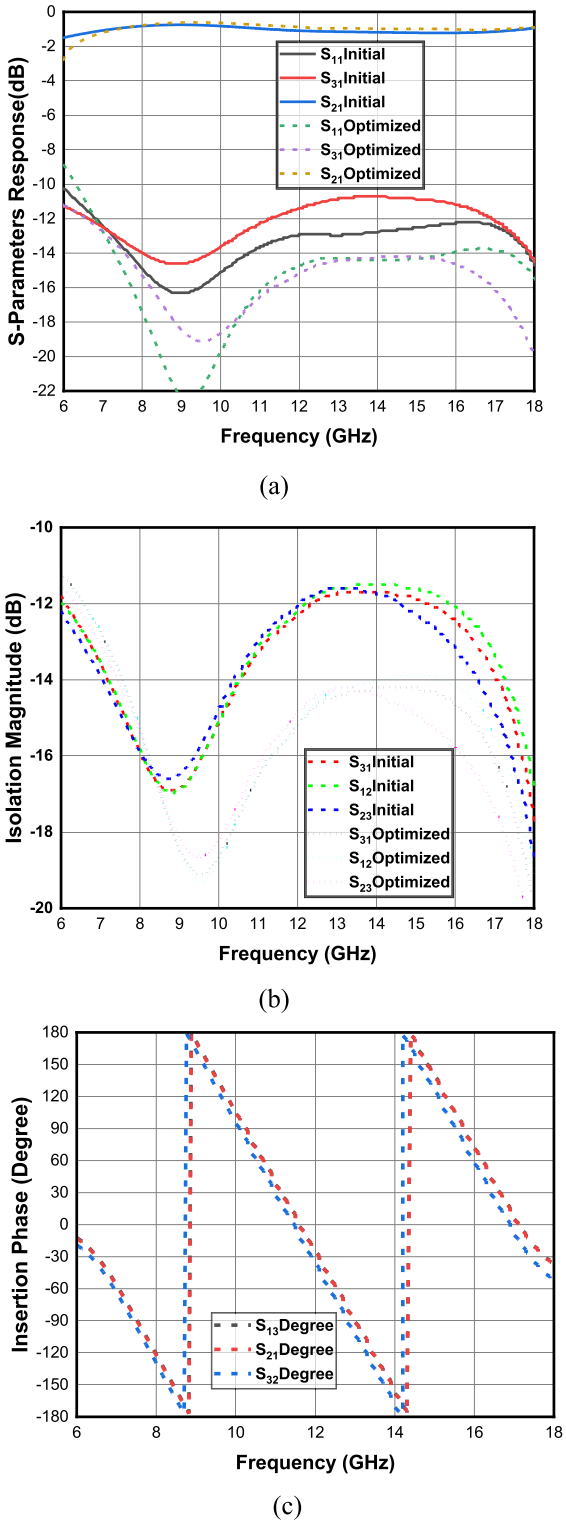

FIGURE 8. (a) Graph of initial versus optimized S-parameters of 6-18 GHz circulator; (b) graph of initial versus optimized isolation at each port; (c). simulated phase different among the ports.

The design specifications fall into the AR region, and the value calculated using (1) for the saturation magnetization of the circulator is 435 G. For this design, the same procedure

TABLE 6. Optimized design parameters and results for the wideband strip-line circulator at a frequency of 12 GHz.

Parameter	Value
Saturation magnetization ($4\pi M_s$)	3800 G
Resonance linewidth (ΔH)	200 Oe
Ferrite radius (R)	2.11 mm
Ferrite thickness (d)	1.52 mm
Inner strip-line width ($W1$)	1.16 mm
Bandwidth (BW)	12 GHz
Insertion loss (IL)	0.42 dB
Return loss (RL)	15 dB
Isolation (IS)	14 dB

TABLE 7. Design specifications for the 1.4–1.6 GHz circulator.

Specification	Value
Lower frequency	1.4 GHz
Upper frequency	1.6 GHz
Bandwidth	0.2 GHz
Insertion loss (IL)	0.4 dB
Isolation (IS)	20 dB
Return loss (RL)	19 dB

can be applied to find the other major parameters of the ferrite, but it needs some modification on biasing. In this case, $\mu = 1$, $\kappa = f_m/f_0 = 0.6222$ and therefore μ_{eff} and k_{eff} are calculated as $\mu_{eff} = (\mu^2 - \kappa^2)/\mu = 0.6128$ and $k_{eff} = \omega\sqrt{\varepsilon_f \mu_{eff}} = 100.013$. In this case, $k_{eff}A = 3.68$ is applied for triangular center conductor geometry. Using (9), $Q_L = 0.71/(\kappa/\mu) = 1.141$ and various combination of $S_{\max}$ & $S_{\min}$ up to 1.10, that is corresponding to $0.065 < G_R < 0.10$. For $1.13 < G_R < 1.5$ and max VSWR, the value of G_R is selected to be 0.075. Next, using (8), single ferrite thickness is calculated $d = 5.012$ mm. Wave admittance is calculated to $Y_{eff} = 0.0178$ and coupling angle $\psi = 0.52$ rad is derived from(10). Finally, the inner strip-line width is then calculated using (12). After the whole analysis and calculation, we selected yttrium iron garnet (YG04) ferrite from Ningbov Chiyue [57] for this design, and its customized parameters are summarized in Table 8.

TABLE 8. Electrical parameters of ferrite at 1.4–1.6 GHz.

Parameter	Value
Saturation magnetization ($4\pi M_s$)	400 G
Resonance linewidth (ΔH)	50 Oe
Ferrite dielectric constant (ε)	13
Land-g factor (g)	2
Ferrite radius (R)	16.5 mm
Ferrite thickness (d)	5 mm

The Y-junction parameters are calculated using the same procedure as in the previous section, which the equation (17) is applied and followed by mentioned method to get electrical dimensions of strip-line. The problem arising when designing a circulator to operate at a low frequency is its size. One of the solutions to this issue is to use a complex center conductor. In this case, a triangular center conductor geometry is selected as it can reduce the thickness of the ferrite by one third of the disk radius. Figure 9 shows a Y-junction strip-line with a triangular center conductor. At a low frequency, the calculated value of the inner width is large, meaning that the triangular shape almost covers the inner width of the strip-line. In this design, air is used as a dielectric material. If the goal is to miniaturize the device, a material with a high dielectric constant can be used. The triangular with a small extended edge Y-junction conductor tends to match well with 50 Ω connectors according to the simulation. Here, we can plot the impedance and admittance in Smith Chart and compare the results. The normalized load admittance $Y_L = 1/Z_L = 1.0561\text{-j}0.62559$ for the triangular shape conductor while $Y_L = 1/Z_L = 1.0115\text{-j}0.2568$ or the circular conductor. Normally, the circulator is connected to 50Ω load connectors. Theoretically, impedance matching is designed when the load impedance equals the complex conjugate of the source impedance. However, to match the Y-junction circulator at circulation frequency (f_0), the conjugate of Z_0, noted by (Z_0^*), must be matched by the access line loaded by 50 Ω. In this case, f_0 and Z_0 are purely real, while characteristic impedance is a complex number.

So, the extended edge of the triangular center conductor has characteristic admittance of $Y_s = 0.0446\text{-j}0.36879$. To get the final dimension of 1.4 –1.6 GHz Y-junctions strip-line, the initial dimensions has been optimized in HFSS simulation. The final dimensions of the Y-junction center conductor are shown in Table 9.

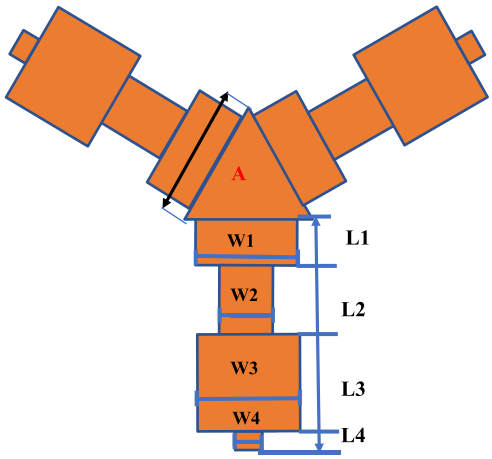

FIGURE 9. Y-junction strip-line for the 1.4–1.6 GHz circulator.

Figure 10 shows a comparison between a disk and a triangular center conductor. The triangular conductor provides an isolation (S_{31}) of 20 dB and a return loss (S_{11}) of 19 dB at the upper and lower frequencies, which meets the design requirements, while the circular conductor is only 1 dB lower. Either of these two configurations can therefore be used, but for this design, we select a triangular shape. The reason for this is that the extended shape acts as a matching stub that

TABLE 9. Parameters of the 1.4-1.6 GHz Y-junction strip-line.

Parameter	Value
Center conductor altitutude (A)	8.5 mm
Inner width ($W1$)	12 mm
First section width ($W2$)	6.02 mm
Second section width ($W3$)	12 mm
Third section width ($W4$)	3.01 mm
Inner section length ($L1$)	10 mm
First section length ($L2$)	8 mm
Second section length ($L3$)	10.95 mm
Third section length ($L4$)	2.25 mm

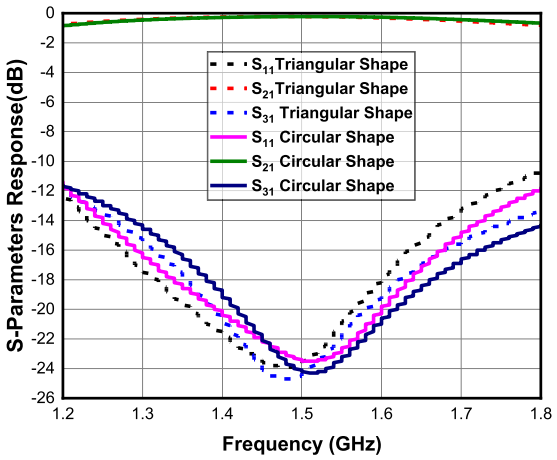

FIGURE 10. Results from a simulation of S-parameters response for triangular and circular center conductors.

can cancel the imaginary part of the complex impedance of the ferrite resonator. Finally, the circulation conditions of the triangular and circular center conductors are depicted in Fig. 11 (a) and (b) respectively, where the axial electric field distributions for each case are plotted. It can be observed that the field circulates from port 1 to port 2 in a clockwise direction, while very little of the field penetrates to port 3. The figure also shows that the maximum electric field distribution for the triangular shape is less than for the circular shape by 0.23×10^4 V/m. These slight drops in the magnitude of the electric field will increase the isolation at port 3 and improve the power handling capability.

The difference between BR and AR circulator is the amount of bias field that is applied. An AR circulator requires a huge biasing field to avoid low loss. In this case, the internal biasing field is found to be five times the saturation magnetization ($4\pi M_s$), resulting an internal magnetic field is $(H_{in}) = 1996$ Oe, using (19). Next, we substitute into (20) to find the (H_0) that can be used to design a magnetic circuit. The thickness and diameter of the applied external magnet were derived as followed mentioned procedure in the BR circulator. Using Maxwell3D simulation, the final magnet's dimension is obtained in Table 10. A rare earth magnet (NdFeB-N35) from SMD magnetic is used [58]. In addition, the direction of the electromagnetic waves under biased

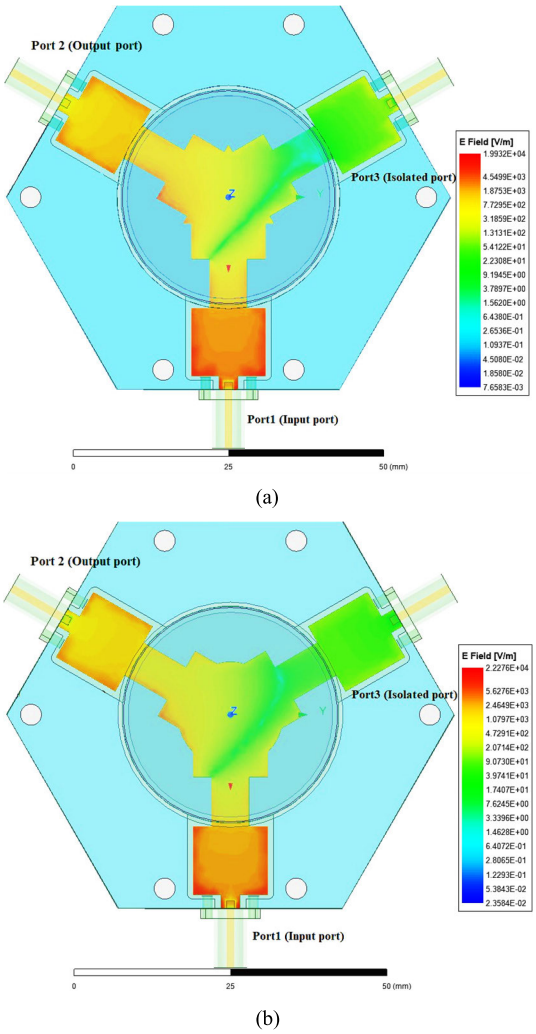

FIGURE 11. Axial electric field at a center frequency of 1.5 GHz: (a) triangular center conductor; (b) circular center conductor.

TABLE 10. Technical properties of neodymium-iron-boron grade N35 for an AR circulator.

Parameter	Value
Intrinsic coercive force (H_{ci})	12 kOe
Residual induction (B_r)	11.8 kG
Grade	N35
Maximum energy product ($BH_{\max}$)	35 MGOe
Curie temperature (T_c)	350 °C
Maximum operating tempearute (T_m)	80 °C
Magnet diameter (D)	34.54 mm
Magnet thickness (d)	4 mm

scheme (clockwise or anti-clockwise) is observed. The pole of a magnet is observed as depicted in Fig 12. The magnet's north pole always points up, in the clockwise direction. And south pole always points down and vice versa if in the anti-clockwise order.

In addition, external magnetic field biasing also contributes to providing high isolation in the right frequency band. In this

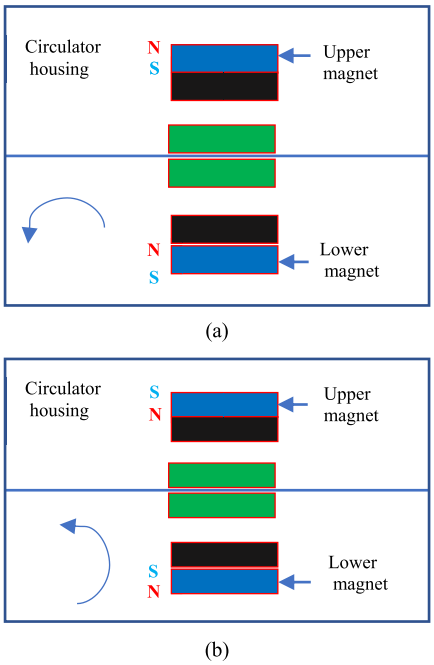

FIGURE 12. Direction of external biased of permanent magnets; (a) clockwise biased; (b) anti-clockwise biased.

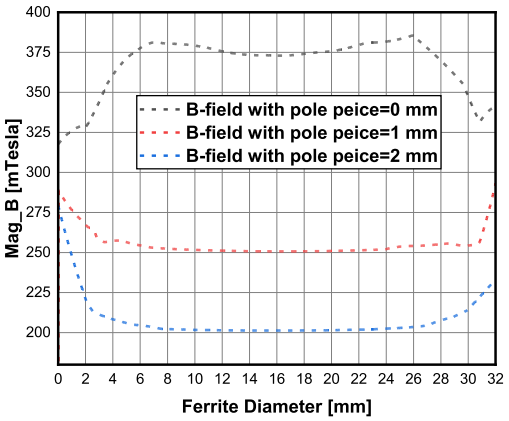

FIGURE 13. Difference in the magnetic fields inside the ferrite due to changes in the pole piece thickness for a 1.4–1.6 GHz strip-line circulator.

case, the magnetic field (*B*-field) in the ferrite is observed using magnetostatic simulation, with the pole piece as the changing variable. The maximum and minimum internal fields in the ferrite with a pole piece of 1 mm, calculated as a *B*-field from post-processing in Maxwell3D, were 250 and 330 mT, respectively, as shown in Fig. 13. These values provided an isolation value of below 20 dB at a center frequency of 1.5 GHz. Using a pole piece of thickness 2 mm, the B-field dropped to 50 mT below that for the 1 mm pole piece. When the pole piece was removed, the internal magnetic field (*B*-field) was reversed, with a maximum at the center of the ferrite and a minimum at the edge of the ferrite. The maximum and minimum internal magnetic fields also increased, leading to a shift in the frequency band (1.6 to 2 GHz) outside of our design requirements. However, in the simulation, this issue can be solved by slightly decreasing the diameter of the permanent magnet or reducing the saturation of the ferrite. In reality, the pole piece should be used to provide a ground plan for the magnet and to offer the possibility of adjustment during assembly and measurement.

IV. FABRICATION AND TESTING

Two prototype Y-junction strip-line circulators were fabricated. A photograph and the performance of each circulator are illustrated in Figs. 15 and 16. All circulators were measured with an Agilent Technologies E8363C PNA Network Analyzer. Before the commencement of the measurement process, the PNA Network Analyzer needs to be calibrated to offset any systematic errors. The calibration process is conducted with the full two ports calibration model through the coaxial Short Open-Load-Thru (SOLT) calibration method, using the Agilent 85052D Economy Mechanical Calibration Kit. The circulator's prototype measurement can be summarized as shown in Fig. 14.

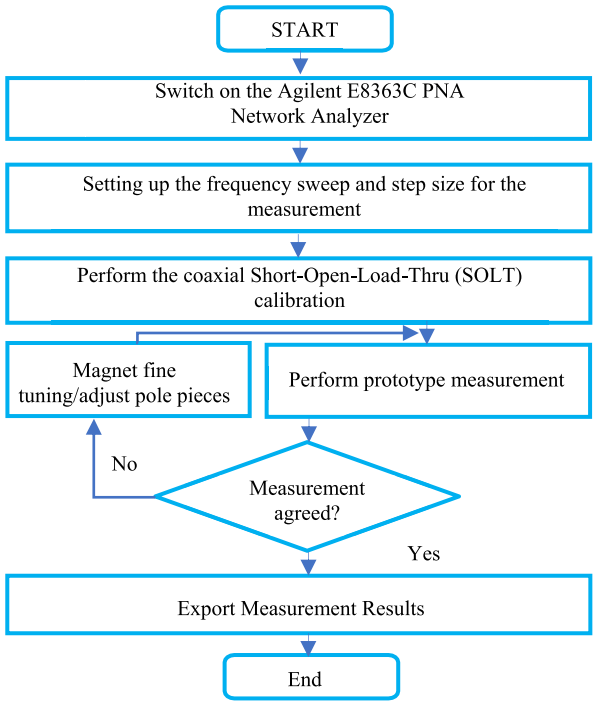

FIGURE 14. Flow chart of prototypes measurement.

Figures 15 (b) and 16 (b) depict a performance of each circulator. These results are also compared to an EM simulation using a 3-D model in HFSS. Figure 15(b) shows a comparison between the simulated and measured S-parameter response for the 1.4–1.6 GHz strip-line circulator. It shows a measured isolation (S_{21}) of 19.4 dB and a return loss (S_{11}) of 25.3 dB at the 1.5 GHz center frequency, values that agree well with those from the simulation. The performance of the narrowband circulator at the band edge compared to the simulated results due to the use of a manual adjustment to the strength of the permanent magnet to track for correct performance. The measurement results for the wide-bandwidth circulator

TABLE 11. Comparison of the proposed wide-bandwidth circulator with some previously published works.

Ref	Frequency (GHz)	Fabrication technology	BW (%)	IL (dB)	ISO (dB)	RL (dB)
This work	10-16	Strip-line	46.2	0.25	12.2	22.4
[59]	4.5-10.5	Strip-line	80	0.37	22	21
[34]	8-12.5	Strip-line	41.6	N/A	15 (Sim)	15 (Sim)
[12]	7.46-12.06	Microstrip line	47	0.6	25	24
[29]	7-15	Microstrip line	72.7	1	15	N/A
[35]	12-18	Ridge gap waveguide (RGW)	40	1.5	20	20

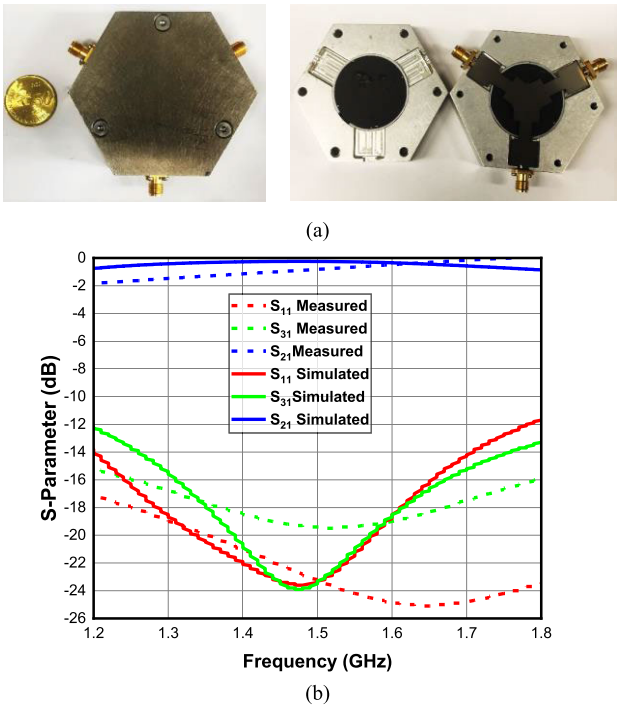

FIGURE 15. (a) Photograph of the 1.4–1.6 GHz narrowband circulator; (b) simulated and measured performance of the narrowband circulator for S_{11}, S_{21}, and S_{31}.

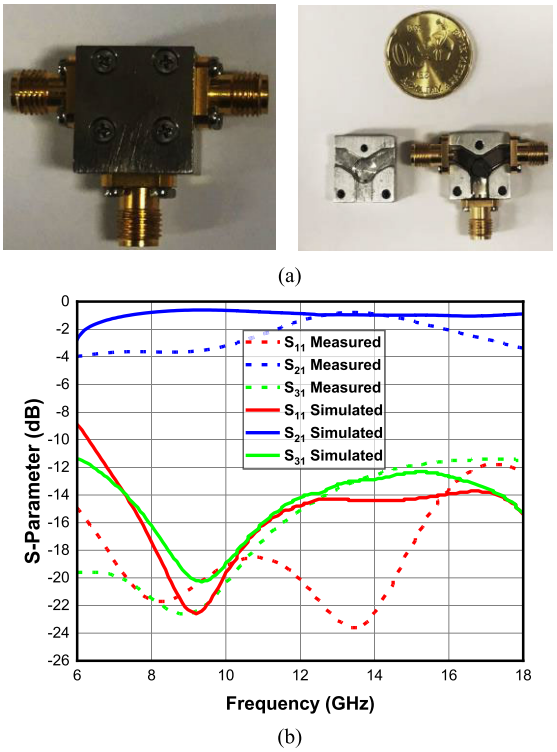

FIGURE 16. (a) Photograph of the 6–18 GHz wideband circulator; (b) simulated and measured performance of the wideband circulator for S_{11}, S_{21}, and S_{31}.

plotted in Fig. 16(b) show a wide range of operation from 6–18 GHz, with values for the isolation (S_{31}) below 11 dB in band of 6-18 GHz. The insertion loss (S_{21}), isolation (S_{31}) and return loss (S_{11}) are 0.25, 12.2 and 22.4 dB, respectively at frequency 14 GHz. A fractional bandwidth of greater than 46% and an isolation of 11 dB were obtained from the experimental results for the wide-bandwidth circulator as shown in Fig. 15 (b). We noticed a slight downwards drift in the insertion loss (S_{21}) between the simulated and measured performance both Fig. 15(b) and 16(b). For example, the measured insertion loss (S_{21}) for the narrowband circulator is around 1 dB, and the insertion loss (S_{21}) of the wideband circulator fluctuates around a value 2.5 dB lower than the simulated results. This is due to the overall losses arising from the SMA connector, RF cable, and the magnetic loss.

V. POWER HANDLING CAPABILITY OF THE CIRCULATOR

The power handling capability of circulators is an essential aspect of transmitter and receiver systems. Unlike other passive circuit devices, the power handling of circulators can be divided into two modes: peak power and average power. Their maximum power handling can be determined by the heating in the materials (related to the conductor, dielectric, and magnetic losses), which limits the average power handling capability, and by the dielectric breakdown field strength (related to the maximum peak voltage that the dielectric can withstand under the worst conditions) which limits the peak power handling capability [61], [62], [63], [64], [65], [66], [67]. Circulators destined for operation in space or other high-vacuum applications may be susceptible to multipaction and other problems, such as nonlinear effects in the material [43], [44]. An excessive peak power leads to corona and arcing, due to the high voltage that can be present. Factors such as the conductor losses in the ferrite set a lower limit on the specifications for the insertion loss of the circulator. It can be seen that circulators designed to handle high power levels will require a low insertion loss to minimize the amount

TABLE 12. Comparison of the proposed narrow-bandwidth circulator with some previously published works.

Ref	Frequency (GHz)	Fabrication technology	BW (%)	IL (dB)	ISO (dB)	RL (dB)
This work	1.4–1.6	Strip-line	13.4	1.5	19.4	25.3
[15]	10.5–13.5	Strip-line	25	2	24	23
[60]	1.643–2.027	Strip-line	20.9	N/A	N/A	N/A
[51]	3.3–4.3	Strip-line	26.3	0.36	23	20
[32]	4–4.8	Microstrip line	13.6	2.5	30	25
[30]	5.7–6.46	Microstrip line (3D printed)	12.5	0.76	15	21
[33]	10–14	Empty substrate integrated coaxial line (ESICL)	33.3	1	10	10
[24]	11–13	Wave guide technology	16	N/A	30 (Sim)	26 (Sim)

of power dissipated in the circulator in the form of heat. The power handling of a circulator cannot exceed the capacity of the waveguides or connectors that interface with it, but in many cases the basic structure of circulator itself will limit the power handling. Waveguide circulators have high power handling performance than strip-line circulators [68], [69]. Some strip-lines circulators from industrial specifications have power handling around 10 W on average, and the peak power is limited to the power of connector itself. Microstrip lines and microstrip circulators have lower power handling than their counterparts.

A. PEAK POWER HANDLING

Strip-line circulators have optimum power handling and are easily integrated with other systems by means of various connectors that are available on the market. Their power handling characteristics can be derived from the strip-line circuit [62]. Properly designed strip-line circulators are capable of handling reasonable power levels, although they will never approach the capabilities of waveguides or even coaxial lines of comparable cross-section. The failure mechanism at peak power is arcing or ''breakdown''. The conditions which cause this vary widely, and include field concentrations as well as airgaps and sharp edges, which serve as field concentrators. The correlation between breakdown and peak power handling for a microwave resonator [63] is also found to be applicable to a ferrite circulator. A ferrite circulator can be considered as a resonator and will resonate at some point when receiving an applied magnetics biasing field. The breakdown power (P_{BD}) of ferrite resonator can be predicted theoretically and simulated of the prototype, which secures the power handling capabilities after fabrication. Peak power is a power that is below the breakdown (P_{BD}) power, otherwise breakdown may occur. A method of normalization to 1 nJ of stored energy in the cavity was proposed in [67]. In this approach, the maximum normalized E-field strength ($E_{Max,norm,peak}$) in the cavity (ferrite resonator) is used to find normalized power, that is put in simulation to achieve 1 nJ stored energy. Then, from [42] and [48], the breakdown power of the ferrite resonator is derived as (31):

$$E_{BD,peak} = E_{Max,norm,peak}\sqrt{P_{BD}EP}. \tag{29}$$

This gives:

$$P_{BD} = \left(\frac{E_{BD,peak}}{E_{Max,norm,peak}}\right)/EP. \tag{30}$$

The calculation of the breakdown threshold (E_{BD}) was discussed in [65]. The author used a set of equations to calculate the breakdown threshold semi-analytically. RF and microwave engineers always use a semi-analytical approximation to calculate the breakdown threshold, since the geometrical structure in the cavity is complicated in practice. Usually, a rule of thumb is used by microwave engineers with a threshold value of $E_{BD} = 2.28$ MV/m (rms, root mean square) or $E_{BD} = 3.22$ MV/m (peak) in an inhomogeneous structure or $E_{BD} = 2.60$ MV/m (rms) in a homogeneous structure. Both are calculated under atmospheric conditions (1 atm, 760 Torr). To calculate the breakdown power, the maximum E-field strength (E_{Max}) and group delay of the circulator are needed; these values can be easily obtained using EM simulation software (HFSS). In (30), the value of the peak breakdown is calculated. This value indicates the property of the ferrite resonator cavity, i.e., how much power it can handle. If the power exceeds this value, there is a high probability of activating breakdown or somehow lead to ionization breakdown. The suggested procedure for calculating the peak power handling of a ferrite resonator, using the correlation between HFSS and the concept of breakdown, can be summarized as follows:

1) Identify the sensitive component that has a major breakdown as a variable to study.
2) Use the field calculator in Ansys HFSS to calculate the stored energy in the ferrite resonator.
3) Compute the edited source by normalizing the stored energy found in step 2 based to 1 nJ.
4) Find the normalized value for the input of circulator and repeat step 2 to ensure that this time the stored energy is 1 nJ.
5) Plot the complex magnitude of the electric field in the resonator (ComplexMag E-field) using the post-processing tool in HFSS, where the highest value is ($E_{Max,norm,peak}$).
6) Normalize the 50 Ω load to one port of the circulator and plot the group delay of the circulator (i.e., the time

taken by the applied RF signal to travel from the input port to the output port of the circulator).

7) Find the breakdown power using (30). From simulated and experimental results, air is found to have a lower field strength than nickel-zinc ferrite. This is an indication that the air inside the circulator tends to cause a major breakdown for the whole structure. The maximum values of the electric field for the breakdown of air and nickel-ferrite are $E_{BD} = 2.28$ MV/m (rms) [63] and 163.79 MV/m (rms) [70], respectively.
8) Multiply the computed value found in step 7 by $10^{-}9$ to get the final breakdown power.
9) Inject the found peak power to the input port of the circulator and check the electric field (E-field) strength of the ferrite resonator to verify the breakdown electric field strength.

Using the guidelines summarized in above part and full wave 3D, the post simulation results simulation of the 6–18 GHz strip-line circulator are calculated and summarized in Table 13.

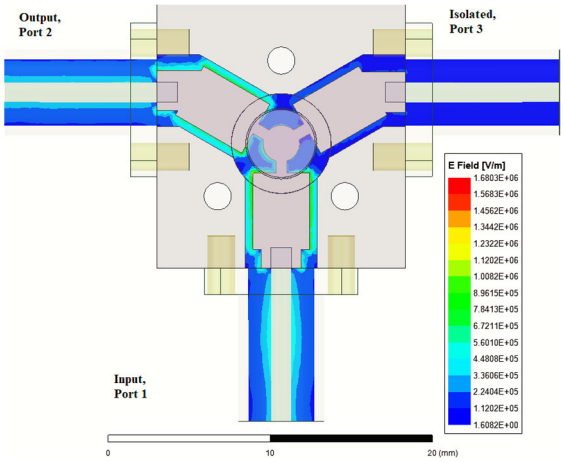

FIGURE 17. Electric field distribution of the Y-junction strip-line circulator at 870.23 W peak power.

TABLE 13. Post simulation results of breakdown calculations.

Parameter	Value
Maximum normalized E-field strength in cavity ($E_{Max,norm,peak}$)	2.37×10^5 v/m
Peak breakdown voltage of air (E_{BD})	3.22×10^6 v/m
Group delay (EP),simulated	0.2127 ns

From (30), the peak power of this strip-line circulator is found to be $P_{BD} = P_{peak} = 870.23$ W. The results of calculation and simulation show good agreement. The peak power flow of the 6–18 GHz strip-line circulator is shown in Fig. 17, where the injected power is 870.23 W. This peak power will guarantee the breakdown power in air. It can be seen that there is a high E-field strength at the place where air is present, which can cause a major breakdown. A well-designed circulator with a higher peak power can be achieved if the airgap is minimized or by using a dielectric material with a high breakdown field strength. The figure also shows that the simulated E-field strength is 1.68 Mv/m, which is slightly higher than half of the breakdown voltage in air, 3.22 Mv/m.

B. AVERAGE POWER HANDLING

The average power handling of a passive circuit such as a microstrip was first studied in [71]. The average power handling of a strip-line was also studied in detail in [62]. The average power handling capability of a planar transmission line is determined by the temperature rises in the conductor and the supporting dielectric material. The losses in the Y-junction strip-line and the microstrip ferrite circulator can be categorized into three main types: dielectric, conductor, and magnetic losses [72].

The procedure for calculating the average power handling capability of most RF devices, including microstrip lines, strip-lines, couplers, and circulators, is the same. Unlike other RF components, the average power handling of a circulator is a little more challenging due to the complex structure and nonuniform behavior of the ferrite material. The calculation for the ferrite circulator starts with the calculation of the conductor and dielectric losses, which can be found in [62]. Normally, the magnetic loss is assumed to be constant, and its value is derived from the material supplier's datasheet. The heat flow distribution over the circulator cross-section is derived to obtain the temperature rise of each component in the circulator except the metal housing. The free space radiation occurs towards both sides of ground plane, while the path length may be shorter toward strip-line or ferrite and then, longer toward. A simple technique that makes use of the concept of thermal resistance permits a reasonable calculation of the temperature rise in the strip-line center conductor. If we take each of the interfaces of the conventional line and determine the temperature drop from interface to interface, as shown in Fig. 18, then the thermal rise in the center conductor can be calculated from (31). Finally, the maximum average power for the strip-line circulator may be calculated using (32).

$$\Delta T_{(N,N+1)} = \frac{(R)(L)(P)}{A} \tag{31}$$

where A is the cross-section of the heat flow path (m^2)
L is the path length (m)
$R = 1/K$ is the thermal resistivity (°C.m/W)
P is the dissipated power (w)
$\Delta T_{(N,N+1)}$ is the thermal rise from one structure to [72] another (°C/W)

As shown in Fig. 19, each layer has its own dissipated power and thermal rise. The power dissipation is the result of the conductor loss (α_c), dielectric loss (α_d), and magnetic loss (α_m), and has units of (dB/unit length) [61], [62], [72]. Once the total thermal rise (ΔT) is known, the maximum average

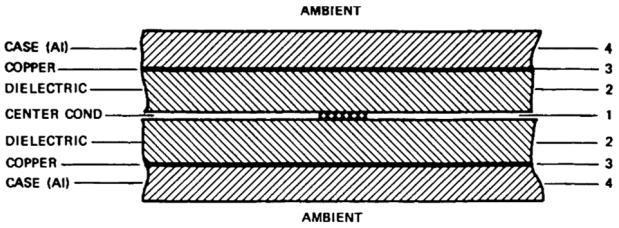

FIGURE 18. Cross-section of line construction used for the thermal analysis curves [62].

power (P_{MAX}) is obtained using (33):

$$P_{MAX} = (T_{MAX} - T_{AMB})/\Delta T \tag{32}$$

where T_{MAX} is the maximum operating temperature of the proposed structure and is defined in the datasheet. T_{AMB} is a set of given constants, and 25°C is a typical value for laboratory measurements. The procedure used to calculate the average power of the strip-line circulator can be summarized as follows:

1) Define all related strip-line circulator parameters under study (operating frequency, dielectric constant, ferrite thickness, width, and height, etc.).
2) Calculate the conductor, dielectric, and magnetic loss of the circulator. The conductor and dielectric loss can be found using the formula stated in [62] or can be read from a graph. The magnetic loss is a constant, and its value is available from the ferrite supplier's datasheet. In this step, a full-wave simulator can be used to find these losses accurately.
3) Identify the heat flow field properties of each material, i.e., the thermal conductivity, path length and cross-section of the structure, as shown in Fig. 18.
4) Calculate the thermal rise in each part of the circuit using (31). The thermal conductivity of the metal housing is higher than 100 W/m°C, which results in lower thermal resistance, and its thermal rise may be negligible. Three main components with huge thermal rises are the ground plan, tracing conductor and ferrite resonator.
5) Define the maximum operation and surrounding ambient temperature of the circulator under study. Based on the total thermal rise found in step 4, the maximum average power is found using (32).

For our analysis of the average power handling of this circulator, we refer to [61], [62], [71]. The total thermal rise in the structure is calculated as 3.90 °C/W. The maximum operating temperature of the circulator should be such that the electrical, magnetic, and physical characteristics remain unchanged. For this calculation, maximum operation, and surrounding temperatures of 85 °C and 20 °C are assumed. The maximum average power is found to be 13.13 W using equation (32).

To validate the proposed procedure, a power handling of 6–18 GHz strip-line circulator was simulated using Icepak,

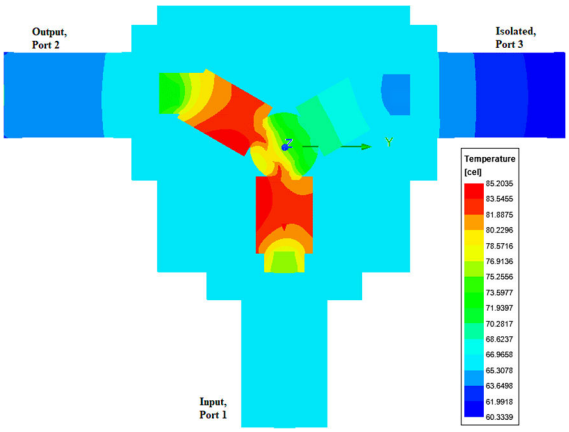

FIGURE 19. Simulated thermal analysis of a strip-line junction circulator at 13.13 W average power, using Ansys Icepak.

an electronic thermal management and thermal analysis software package. The simulation was carried out using HFSS in conjunction with Icepak, for an input power of 13.13 W at port 1. Here, the maximum temperature was found to be 85.20 °C, indicating a good match between calculation and simulation, as shown in Fig. 19. This verifies the value of 13.13 W of the maximum average power handling of the circulator in calculation. The highest temperature occurs in the Y-junction conductor, where there is the maximum electric field, since at an operation frequency of 12 GHz the conductor losses predominate over the dielectric and magnetic losses. In the circulator, the power is transferred from the input (port1) to the output (port 2), while isolating port 3. Most of the power goes from port 1 and exist port 3, resulting in the maximum temperature being located between ports 1 and 2.

The average power handling of the circulator depends upon the thermal conductivity of the material, the transmission line loss of the Y-junction, the magnetic loss of the ferrite, and the ambient temperature, which determine the maximum average power handling capability. In the view of the thermal effect on the maximum average power handling capability, the surrounding temperature may be higher than the ambient temperature, leading to power handling that is much lower than average. Fig. 20(a) and (b) show the downward drift in temperature in the whole circulator as the external factors like casing material and surrounding temperature varies. Increasing the surrounding temperature results in lower power handling while maintaining the temperature below the maximum operation temperature, as shown in Fig. 20(a). An aluminum metal housing is better for a high-power circulator due to its high thermal conductivity (200 W/m°C), low cost, weight, and high resistance to corrosion. External factors such as the selection of a material with high thermal conductivity and a proper cooling method also play an important role in the power handling capability of a strip-line circulator. Cold-rolled steel has a lower thermal conductivity (51.9 W/m°C) and is often used as a metal casing due to its ability to confront the magnetic shielding and sometime act as a return path

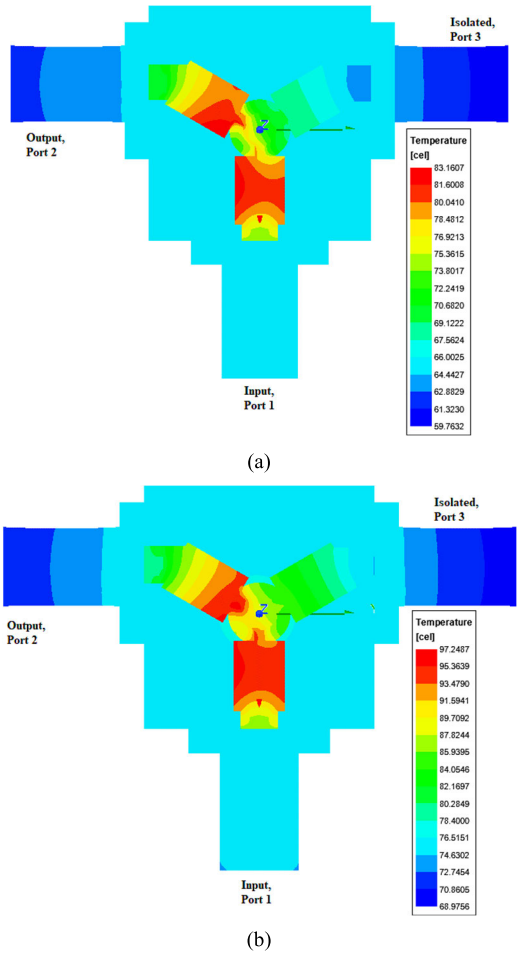

FIGURE 20. Simulated thermal profile generated by adjusting external factors: (a) surrounding temperature 25 °C; (b) using cold-rolled steel as a casing material.

to complete magnetic circuit. Fig. 20(b) shows simulation results for the temperature of a cold-rolled steel metal casing, which is 12.05°C higher than for aluminum. In a practical circulator, a combination of these two metals should be considered to minimize this effect. For example, aluminum may be used for the bottom and top ground planes, and cold-rolled steel for the upper and lower pole pieces, to improve the magnetic shielding and ensure a good power handling capability.

VI. CONCLUSION

In this work, the key design equations for a circulator are addressed. Our analysis shows that the proposed enhanced closed form expression can generate all the required circulator parameters, which are sufficient for a complete EM simulation. In addition, a semi-analytical approach provides a satisfactory S-parameter response compared to the conventional design approach and can be applied to the design of a circulator operating in both BR and AR modes, with a few modifications to the matching and biasing field. Two prototypes of strip-line junction circulators were designed, fabricated, and evaluated to validate the proposed concept. It is expected that with suitable external biasing and practical assembly, the overall performance of these prototype circulators can be improved. In addition, the power handling capabilities of the circulators were analyzed and studied. A completed EM simulation of the power handling capabilities of ferrite circulator was conducted to validate theoretical analysis. The selection of a suitable ferrite material and the environmental surroundings play an important role in power handling for realistic applications.

REFERENCES

[1] T.-H. Chang, "Ferrite materials and applications," in *Electromagnetic Materials and Devices*, 2020, pp. 1–14, doi: 10.5772/intechopen.84623.
[2] W. V. Aulock, "Selection of ferrite materials for microwave device applications," *IEEE Trans. Magn.*, vol. MAG-2, no. 3, pp. 251–255, Sep. 1966.
[3] M. D. Hill, D. B. Cruickshank, and I. A. MacFarlane, "Perspective on ceramic materials for 5G wireless communication systems," *Appl. Phys. Lett.*, vol. 118, no. 12, Mar. 2021, Art. no. 120501, doi: 10.1063/5.0036058.
[4] V. Voronkov, "Microwave ferrites: The present and the future," *Le J. Phys. IV*, vol. 7, no. C1, pp. C1-35–C1-38, Mar. 1997, doi: 10.1051/jp4:1997104.
[5] V. G. Harris, A. Geiler, Y. Chen, S. D. Yoon, M. Wu, and A. Yang, "Recent advances in processing and applications of microwave ferrites," *J. Magn. Magn. Mater.*, vol. 321, no. 14, pp. 2035–2047, 2009.
[6] H. Bosma, "On the principle of stripline circulation," *Proc. IEE-B, Electron. Commun. Eng.*, vol. 109, no. 21, pp. 137–146, Jan. 1962.
[7] H. Bosma, "A general model for junction circulators; choice of magnetization and bias field," *IEEE Trans. Magn.*, vol. MAG-4, no. 3, pp. 587–596, Sep. 1968.
[8] H. Bosma, "On stripline Y-circulation at UHF," *IEEE Trans. Microw. Theory Techn.*, vol. MTT-12, no. 1, pp. 61–72, Jan. 1964.
[9] C. E. Fay and R. L. Comstock, "Operation of the ferrite junction circulator," *IEEE Trans. Microw. Theory Techn.*, vol. MTT-13, no. 1, pp. 15–27, Jan. 1965.
[10] C. M. Krowne, "Theory of the recursive dyadic green's function for inhomogeneous ferrite canonically shaped microstrip circulators," *Adv. Imag. Electron Phys.*, vol. 98, pp. 321–377, Jan. 1996.
[11] J. Lee, Y.-K. Hong, C. Yun, W. Lee, J. Park, and B.-C. Choi, "Magnetic parameters for ultra-high frequency (UHF) ferrite circulator design," *J. Magn.*, vol. 19, no. 4, pp. 399–403, Dec. 2014, doi: 10.4283/jmag.2014.19.4.399.
[12] V. V. K. Thalakkatukalathil, A. Chevalier, V. Laur, G. Verissimo, P. Queffelec, L. Qassym, and R. Lebourgeois, "Electromagnetic modeling of anisotropic ferrites—Application to microstrip Y-junction circulator design," *J. Appl. Phys.*, vol. 123, no. 23, Jun. 2018, Art. no. 234503, doi: 10.1063/1.5026482.
[13] S. Ayter and Y. Ayasli, "The frequency behavior of stripline circulator junctions," *IEEE Trans. Microw. Theory Techn.*, vol. MTT-26, no. 3, pp. 197–202, Mar. 1978.
[14] P. Krivic, G. Radosavljevic, S. Birgermajer, N. Cselyuszka, and H. Arthaber, "Design and fabrication of the Bosma stripline circulator in LTCC technology," in *Proc. IEEE Int. Conf. Microw., Commun., Antennas Electron. Syst. (COMCAS)*, Nov. 2015, pp. 2–4.
[15] A. Ghadiya, K. Trivedi, S. Soni, and P. Bhatt, "Wide band stripline circulator at Ku band for space applications," in *IEEE MTT-S Int. Microw. Symp. Dig.*, Nov. 2018, pp. 1–7.
[16] Z. Uzdy, "Computer-aided design of stripline ferrite junction circulators," *IEEE Trans. Microw. Theory Techn.*, vol. MTT-28, no. 10, pp. 1134–1136, Oct. 1980.
[17] A. M. Borjak and L. E. Davis, "More compact ferrite circulator junctions with predicted performance," *IEEE Trans. Microw. Theory Techn.*, vol. 40, no. 12, pp. 2352–2358, Dec. 1992.
[18] K. Tian, L. Z. You, and H. Liu, "Minimized Ku band microstrip circulator design," in *Proc. Int. Conf. Microw. Millim. Wave Technol.*, May 2010, pp. 1967–1968.
[19] E. Schwartz, "Broadband matching of resonator circuits and circulators," *IEEE Trans. Microw. Theory Tech.*, vol. MTT-16, no. 3, pp. 158–165, Mar. 1968.

[20] E. Schloemann and R. E. Blight, "Broad-band stripline circulators based on YIG and Li-ferrite single crystals," *IEEE Trans. Microw. Theory Techn.*, vol. MTT-34, no. 12, pp. 1394–1400, Dec. 1986.
[21] A. Setiawan, Y. Y. Maulana, Y. Sulaeman, T. Praludi, and Y. Taryana, "Design of 3 GHz stripline ferrite circulator for radar applications," in *Proc. Int. Conf. Radar, Antenna, Microw., Electron., Telecommun.*, 2017, pp. 154–157.
[22] V. Kelaiya and M. R. Naik, "Design and simulation of X band microstrip circulator," in *Proc. IEEE Region 10 Conf. (TENCON)*, Nov. 2016, pp. 1961–1964.
[23] E. J. Sedek and A. T. Milewski, "Computer aided design and optimization of three-port ferrite stripline and microstrip circulators," *WSEAS Trans. Inf. Sci. Appl.*, vol. 2, no. 9, pp. 395–398, 2005.
[24] H. Ren and Y. Xie, "Simulation design of an X-band high isolation circulator," in *Proc. 2nd Int. Conf. Inf. Technol. Comput. Appl. (ITCA)*, Dec. 2020, pp. 387–390.
[25] D. B. Cruickshank, *Implementing Full Duplexing for 5G*. Norwood, MA, USA: Artech House, 2006.
[26] J. Helszajn, *The Stripline Circulator: Theory and Practice*, 1st ed. Rosewood, MA, USA: Wiley, 2008.
[27] D. M. Pozar, *Microwave Engineering*, 4th ed. Rosewood, MA, USA: Wiley, 2012.
[28] D. K. Linkhart, *Microwave Circulator Design*, D. K. Linkhart, Ed., 2nd ed. Norwood, MA, USA: Artech House, 2014.
[29] J. Rosenbaum and Y. S. Wu, "Wide-band operation of microstrip circulator," *IEEE Trans. Microw. Theory Techn.*, vol. MTT-22, no. 10, pp. 849–857, Oct. 1974.
[30] V. Laur, J. P. Gouavogui, and B. Balde, "C-band hybrid 3-D-printed microwave isolator," *IEEE Trans. Microw. Theory Techn.*, vol. 69, no. 3, pp. 1579–1585, Mar. 2021.
[31] S. A. Ivanov, "Inherently matched Y-junction stripline circulator," *IEEE Trans. Microw. Theory Techn.*, vol. 45, no. 5, pp. 648–652, May 1997.
[32] M. Pinto, L. Marzall, A. Ashley, D. Psychogiou, and Z. Popovic, "Design-oriented modelling of microstrip ferrite circulators," in *Proc. 48th Eur. Microw. Conf. (EuMC)*, Sep. 2018, pp. 215–218.
[33] L. Martinez, V. Laur, A. L. Borja, P. Queffelec, and A. Belenguer, "Low loss ferrite Y-junction circulator based on empty substrate integrated coaxial line at Ku-band," *IEEE Access*, vol. 7, pp. 104789–104796, 2019, doi: 10.1109/ACCESS.2019.2931588.
[34] S. I. Shams, M. Elsaadany, and A. A. Kishk, "Including stripline modes in the Y-junction circulators: Revisiting fundamentals and key design equations," *IEEE Trans. Microw. Theory Techn.*, vol. 67, no. 1, pp. 94–107, Jan. 2019.
[35] S. I. Shams, S. M. Sifat, M. Elsaadany, G. Gagnon, and A. A. Kishk, "Systematic design procedure for Y-junction circulator based on ridge gap waveguide technology," *IEEE Trans. Microw. Theory Techn.*, vol. 69, no. 4, pp. 2165–2177, Apr. 2021.
[36] L. Marzall, D. Psychogiou, and Z. Popovic, "Microstrip ferrite circulator design with control of magnetization distribution," *IEEE Trans. Microw. Theory Techn.*, vol. 69, no. 2, pp. 1217–1226, Feb. 2021.
[37] M. M. M. Ali, S. I. Shams, M. Elsaadany, and K. Wu, "Stripline Y-junction circulators: Accurate model and electromagnetic analysis based on Gaussian field distribution boundary conditions," *IEEE Trans. Microw. Theory Techn.*, early access, Aug. 17, 2022, doi: 10.1109/TMTT.2022.3197161.
[38] Y. Konishi, "A high-power UHF circulator," *IEEE Trans. Microw. Theory Techn.*, vol. MTT-15, no. 12, pp. 700–708, Dec. 1967.
[39] L. Farhat, E. Laroche, G. Martin, J. Puech, C. Miquel-Espana, and F. de Paolis, "High power Ka-band waveguide (WR51) isolator for space applications," in *Proc. 1st Int. Symp. Space Passive Compon.*, Sep. 2013, pp. 1–8.
[40] F. Okada, K. Ohwi, M. Mori, and M. Yasuda, "A 100 kW waveguide Y-junction circulator for microwave power systems at 915 MHz," *J. Microw. Power*, vol. 12, no. 3, pp. 201–207, Jan. 1977.
[41] F. Okada and K. Ohwi, "Design of a high-power CW Y-junction waveguide circulator," *IEEE Trans. Microw. Theory Techn.*, vol. MTT-26, no. 5, pp. 364–369, May 1978.
[42] Y. Okada, Y. Shimada, M. Furuya, O. Myoh, T. Shimoto, and N. Senba, "The ferrite-embedded drop-in circulator for millimeter wave communication systems," in *Proc. 50th Electron. Compon. Technol. Conf.*, May 2000, pp. 188–192.
[43] Y. M. Jain, P. K. Sharma, K. Ambulkar, P. R. Parmar, A. R. Jadhav, and H. V. Dixit, "Steady-state operation of high CW power circulator: Challenges and solutions through simulation and experiments," *IEEE Trans. Plasma Sci.*, vol. 48, no. 5, pp. 1290–1297, May 2020.
[44] Y. Li, H. Wang, J. Yang, and W. Cui, "Multipactor simulation and suppression in high-power ferrite circulators," in *Proc. Joint Int. Symp. Electromagn. Compat., Sapporo Asia–Pacific Int. Symp. Electromagn. Compat.*, Jun. 2019, pp. 449–452.
[45] M. A. Franzi, S. Tantawi, V. Dolgashev, E. Jongewaard, and J. Eichner, "Novel high-power microwave circulator employing circularly polarized waves," *IEEE Trans. Plasma Sci.*, vol. 48, no. 6, pp. 1984–1992, Jun. 2020.
[46] S. Guo, K. Song, Y. Wang, and Y. Pan, "Compact suspension-stripline circulator for high power applications," in *Proc. IEEE Asia–Pacific Microw. Conf. (APMC)*, Dec. 2019, pp. 853–855.
[47] H. Ren, Y. Xie, H. Wei, P. Wu, and L. Dai, "A novel circulator construction with high multipactor threshold and high isolation for aerospace applications," *IEEE Trans. Plasma Sci.*, vol. 50, no. 3, pp. 715–720, Mar. 2022.
[48] M. A. AbdElraheem, S. I. Shams, M. Elsaadany, G. Gagnon, and A. A. Kishk, "High-power circulator: Assembly design and challenges," *IEEE Trans. Microw. Theory Techn.*, vol. 70, no. 10, pp. 4354–4364, Oct. 2022.
[49] H. Ren and Y. Xie, "Determination of anisotropy ratio k/μ for symmetric three-port circulator using transmission line equivalent model," *IEEE Trans. Magn.*, vol. 57, no. 8, pp. 1–6, Aug. 2021.
[50] L. G. Maloratsky, "Understanding coaxial and drop-in circulator and isolator," Tech. Rep., 2004, doi: 10.1016/B978-075067699-1/50013-4.
[51] N. Jaiswal and P. Pradeepkumar, "Ultra-broadband C-band stripline coaxial isolator design," in *Proc. IEEE Indian Conf. Antennas Propogation (InCAP)*, Dec. 2018, pp. 1–4.
[52] J. W. Simon, "Broadband strip-transmission line Y-junction circulators," *IEEE Trans. Microw. Theory Techn.*, vol. MTT-13, no. 3, pp. 335–345, May 1965.
[53] J. L. Young, R. S. Adams, B. O'Neil, and C. M. Johnson, "Bandwidth optimization of an integrated microstrip circulator and antenna assembly: Part 1," *IEEE Antennas Propag. Mag.*, vol. 48, no. 6, pp. 47–56, Dec. 2006.
[54] S. A. Ivanov, "Application of the planar model to the analysis and design of the Y-junction strip-line circulator," *IEEE Trans. Microw. Theory Techn.*, vol. 43, no. 6, pp. 1253–1263, Jun. 1995.
[55] R. K. Tenzer, "Estimating leakage factors for magnetic circuits by a simple method," in *Applied Magnetics*. Valparaiso, IN, USA: The Indiana Steel Products, Apr./Jun. 1957.
[56] J. M. Camacho and V. Sosa, "Alternative method to calculate the magnetic field of permanent magnets with azimuthal symmetry," *Revista Mexicana física E*, vol. 59, no. 1, pp. 8–17, Jun. 2013.
[57] (2021). *Ningbo Chiyue Import & Export Co. Ltd.* [Online]. Available: https://m.microwaveferrite.com/yig-ferrites-for-isolator-circulator-application-with-the-sintering-temperature-7471391.html
[58] SDM Magnetic. (2004). *Speed, Dedication, Motivation. SDM Magnetics Manufacturers Variety of High Quality Permanent Magnets*. [Online]. Available: https://www.sdmmagnetic.com/discmagnets/magnets/ndfeb/grade/n35
[59] H. Turki, L. Huitema, T. Monediere, B. Lenoir, and C. Breuil, "Complete methodology of low-loss ultra-wideband junction circulator," in *IEEE MTT-S Int. Microw. Symp. Dig.*, Jun. 2018, pp. 746–749.
[60] H.-W. Chao, S.-Y. Wu, and T.-H. Chang, "Bandwidth broadening for stripline circulator," *Rev. Sci. Instrum.*, vol. 88, no. 2, Feb. 2017, Art. no. 024706.
[61] M. Á. Sánchez-Soriano, Y. Querére, V. Le Saux, C. Quendo, and S. Cadiou, "Average power handling capability of microstrip passive circuits considering metal housing and environment conditions," *IEEE Trans. Compon., Packag., Manuf. Technol.*, vol. 4, no. 10, pp. 1624–1633, Oct. 2014.
[62] H. Howe, *Stripline Circuit Design by Harlan Howe*, 3rd ed. Norwood, MA, USA: Artech House, 1974.
[63] Q. Li, "Correlation between simulation and measurement of microwave resonator power handling," Tech. Rep., 2013.
[64] M. A. Sanchez-Soriano, Y. Quere, V. Le Saux, S. Marini, M. S. Reglero, V. E. Boria, and C. Quendo, "Peak and average power handling capability of microstrip filters," *IEEE Trans. Microw. Theory Techn.*, vol. 67, no. 8, pp. 3436–3448, Aug. 2019, doi: 10.1109/TMTT.2019.2919509.
[65] M. Yu, "Power-handling capability for RF filters," *IEEE Microw. Mag.*, vol. 8, no. 5, pp. 88–97, Oct. 2007, doi: 10.1109/MMM.2007.904712.
[66] A. Jain, R. P. Yadav, and S. Kumar, "Design and development of high power variable dual-directional radio frequency coupler," *IET Microw., Antennas Propag.*, vol. 13, no. 14, pp. 2544–2550, Nov. 2019.
[67] F. De Paolis and F. Frezza, "Simplified prediction of peak power-handling capability for stepped-impedance low-pass filters," *IEEE Trans. Microw. Theory Techn.*, vol. 61, no. 3, pp. 1079–1085, Mar. 2013.

[68] H. Razavipour, G. Askari, F. Fesharaki, and H. Mirmohammad-Sadeghi, "A new high-power, dual-band, E-plane, ferrite circulator," in *Proc. IEEE EUROCON*, May 2009, pp. 20–25.
[69] T. Mroz, R. Frender, and J. Michalowski, "S-band below resonance high power circulator search for ferrite material and structure," in *Proc. Int. Conf. Microw., Radar Wireless Commun.*, May 2006, pp. 354–357.
[70] A. M. Pearson, R. D. Curry, K. M. Noel, S. A. Mounter, and K. A. O'Connor, "High voltage breakdown analysis of Nickle-Zinc ferrite double-positive metamaterials," in *Proc. IEEE Pulsed Power Conf. (PPC)*, May 2015, pp. 1–3, doi: 10.1109/PPC.2015.7296891.
[71] I. J. Bahl and K. C. Gupta, "Average power-handling capability of microstrip lines," *IEE J. Microw., Opt. Acoust.*, vol. 3, no. 1, pp. 1–4, Jan. 1979.
[72] R. E. Neidert and P. M. Phillips, "Losses in Y-junction stripline and microstrip ferrite circulators," *IEEE Trans. Microw. Theory Techn.*, vol. 41, no. 6, pp. 1081–1086, Jun. 1993.

SOKHA KHIM was born in Kampong Cham, Cambodia. He received the B.Eng. degree in electrical and electronics engineering, majored in electrical and electronics from Norton University, Phnom Penh, Cambodia, in 2020. He is currently pursuing the M.Sc. degree (by research mode) in electrical and electronic engineering with the Universiti Teknologi PETRONAS, Malaysia. He is also a Graduate Research Assistant (GRA) with the Department of Electrical and Electronic Engineering, Universiti Teknologi PETRONAS. His main research interest includes the design and synthesis of microwave ferrite circulator/isolator and their application in millimeter-wave frequency. He has been working on filter design, directional coupler, impedance matching waveguide adapter, and various passive devices during his studies.

SOVUTHY CHEAB (Member, IEEE) received the B.Eng. degree (Hons.) in electrical and electronic engineering and the M.Sc. and Ph.D. degrees in RF and microwave engineering from the Universiti Teknologi Petronas (UTP). Before going into industry, he worked as a Lecturer with the Electrical and Electronic Engineering Department, UTP teaching electromagnetic theory, communication systems, and RF/microwave related subjects, for six years. He had supervised a total of six Ph.D. and seven master's students. In terms of research, he had secured many national and industry grant projects. He is a technical consultant on the design and synthesis of RF and microwave passive filter and other components for 5G applications and beyond. He is currently working on the design, simulation and fabrication of the RF and microwave narrow band and broadband circulators. He also works as the Technical Director with FILPAL (M) Sdn Bhd. His role includes leading the training division in the company. He has been an Executive Committee Member of the IEEE ED/MTT/SSC Penang Chapter, since 2016, and had been elected as the Secretary of the Chapter, from 2021 to 2022. He served as the Secretary of IMESS 2018, the MTT Technical Chair of IMESS 2019, and the Publication Chair of ICIAS 2020 Conference.

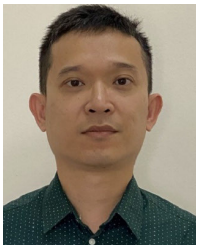

SOCHEATRA SOEUNG (Member, IEEE) was born in Phnom Penh, Cambodia, in 1986. He received the B.Eng. degree (Hons.) in electrical and electronic, major in computer system architecture and the M.Sc. and Ph.D. degrees by research in electrical and electronics engineering from the Universiti Teknologi PETRONAS, Malaysia, in 2010, 2013, and 2018, respectively. From 2014 to 2018, he worked as a Research Officer in RF Microwave Engineer under several Ministry of Higher Education Malaysia and industrial funding projects, while doing his Ph.D. degree. He was involved in designing, implementing, and testing RF subsystem components and RF link. He currently works as a Lecturer and a Computation and Communication Cluster Leader with the Electrical and Electronic Engineering Department, Universiti Teknologi PETRONAS. He has been awarded with several funding as a project principle from Malaysian Government, industries, and University research collaborations. His research interests include RF passive device and circuit, filter design and synthesis, computer-aided tuning, and optimization techniques. He is also an MTT Member and a Committee Member of the IEEE ED/MTT/SSC Penang Chapter, Malaysia.

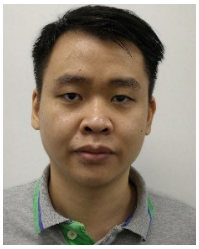

GUAN SHEN NG received the B.Eng. degree in electrical and electronics engineering from the Universiti Teknologi PETRONAS (UTP), Perak, Malaysia, in 2017, fully funded under PETRONAS Education Sponsorship, and the M.Sc. degree in microwave engineering from the Petronas University of Technology, in 2020, under Yayasan Universiti Teknologi PETRONAS (YUTP) Grant. During his studies, he was involved in various narrow-band passive filter design projects, including the design of rectangular waveguide, dual-mode circular waveguide, coaxial and microstrip filters. He has been a Research Officer with UTP, since 2020, and had been working on several RF projects on 5G applications. He currently works as a Research Scientist with the UTP. His research interests include millimeter-wave waveguide filters, 3D metal printing filters, filter miniaturization, and wide spurious-free filters.